Inorganic Chemistry

Article

pubs.acs.org/IC

Ultrafast Intramolecular Charge Separation in a Donor–Acceptor Assembly Comprising Bis(η^5-cyclopentadienyl)molybdenum Coordinated to an Ene-1,2-dithiolate-naphthalenetetracarboxylicdiimide Ligand

Adam J. Taylor,[†] E. Stephen Davies,*[,†] Julia A. Weinstein,*[,‡] Igor V. Sazanovich,[‡] Oleg V. Bouganov,[§] Sergei A. Tikhomirov,[§] Michael Towrie,[∥] Jonathan McMaster,[†] and C. David Garner*[,†]

[†]School of Chemistry, University of Nottingham, Nottingham NG7 2 RD, United Kingdom

[‡]Department of Chemistry, University of Sheffield, Sheffield S3 7HF, United Kingdom

[§]B.I. Stepanov Institute of Physics, Minsk, Belarus

[∥]Central Laser Facility, Science and Technology Facilities Council, Rutherford Appleton Laboratory, OX11 0QX, United Kingdom

Supporting Information

ABSTRACT: The first example of a Donor-spacer-Acceptor tryad, based upon a molybdenum-ene-1,2-dithiolate unit as the Donor and a naphthalene-diimide as the Acceptor, has been synthesized and its photophysical properties investigated. Synthesis required the preparation of a new pro-ligand containing a protected ene-1,2-dithiolate bound through a phenyl linkage to a naphthalenetetracarboxylicdiimide (NDI) group. Deprotection of this pro-ligand by base hydrolysis, followed by reaction with $[Cp_2MoCl_2]$, produced the new dyad $[Cp_2Mo(SC(H)C(C_6H_4{-}NDI)S)]$ (**2**). Electrochemical studies showed that **2** can be reversibly oxidized to $[\mathbf{2}]^+$ and reduced to $[\mathbf{2}]^-$, $[\mathbf{2}]^{2-}$, and $[\mathbf{2}]^{3-}$. These studies, augmented by UV/vis, IR, and electron paramagnetic resonance (EPR) spectra of electrochemically generated $[\mathbf{2}]^+$ and $[\mathbf{2}]^-$, show that the highest occupied molecular orbital (HOMO) of **2** is ene-1,2-dithiolate-based and the lowest unoccupied molecular orbital (LUMO) is NDI-based; these conclusions are supported by density functional theory (DFT) calculations for the electronic ground state on a model of **2** which also showed that these two parts of the molecule are electronically distinct. The dynamics of the excited states of **2** in CH_2Cl_2 solution were investigated by picosecond time-resolved IR spectroscopy following irradiation by a 400 nm ~120 fs laser pulse. These investigations were complemented by an ultrafast transient absorption spectroscopic study from 420 to 760 nm of the nature of the excited states of **2** in CH_2Cl_2 solution following irradiation by a 383 nm ~120 fs laser pulse. These studies showed that irradiation of **2** at both 400 and 383 nm leads to the formation of the $[(Cp)_2\{Mo(dt)\}^+\text{-Ph-}\{NDI\}^-]$ charge-separated state as a result of a cascade electron transfer initiated by the formation of an ^{1}NDI* excited state. ^{1}NDI* rapidly (ca. 0.2 ps) forms the local charge transfer state $[Cp_2Mo(dt)\text{-}\{Ph\}^+\text{-}\{NDI\}^-]$ which has a lifetime of about 1.7 ps and decays to produce the ground state and the charge-separated state $[(Cp)_2\{Mo(dt)\}^+\text{-Ph-}\{NDI\}^-]$; the latter has an appreciable lifetime, about 15 ns in CH_2Cl_2 at room temperature.

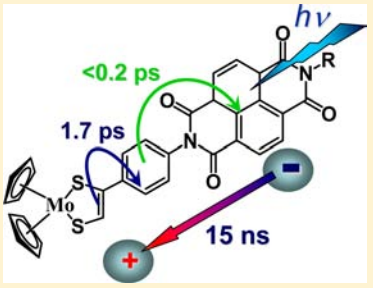

INTRODUCTION

Photoinduced charge separation is a fundamental process which lies at the heart of reactions in natural and artificial systems powered by the energy of light.[1−5] Synthetic dyads and triads, designed to generate an intramolecular charge-separation following the absorption of visible light, usually comprise a chromophore, in which absorption of light quanta generates a local excited state, and at least one additional electron acceptor, electron donor, or both to promote further charge separation in a dark electron transfer cascade.[6] A significant number of the d-transition metal complexes, which possess one (or more) charge-transfer transition(s) of an energy corresponding to that of visible light and are capable of modulation by ligand modification, have been investigated as potential charge-transfer chromophores. Many of these studies have involved d^6 octahedral complexes;[7] also, there have been several investigations of d^8 square planar complexes of Pt(II) and Pd(II).[8−16] Ligands which are capable of reversible redox reactions are particularly important in this context, as the search for photostable light-harvesting systems capable of efficient charge separation continues.

Ene-1,2-dithiolate (dithiolene) ligands generally significantly modify the electronic nature of a metal center through strong covalent interactions and the resultant complexes usually manifest facile redox behavior. Although many ene-1,2-dithiolate complexes have been studied as potential candidates for functional materials with novel optical, magnetic or electrical (e.g., superconductivity) properties,[17−22] there have been relatively few studies that have involved the binding of an

Received: July 3, 2012
Published: September 5, 2012

Scheme 1[a]

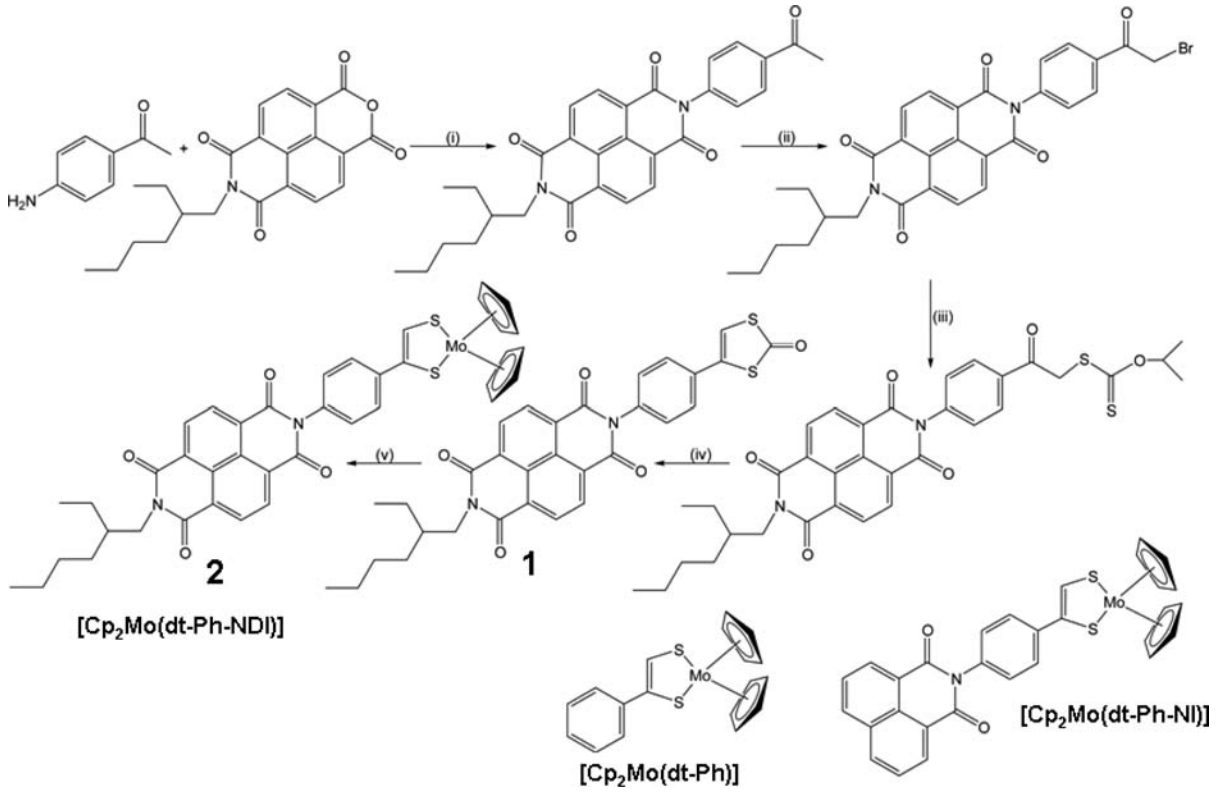

[a](i) DMF, reflux, 24 h., (ii) AcOH/Br_2, 60 °C, 6 h., (iii) potassium *O*-isopropylxanthate, CH_2Cl_2, r.t., 3 h., (iv) H_2SO_4, 5 min, (v) $CsOH{\cdot}H_2O$, MeOH/CH_2Cl_2, r.t., 30 min then $[Cp_2MoCl_2]$, r.t., overnight.

ene-1,2-dithiolate to a transition metal with the aim of producing a complex capable of forming a charge-separated excited state.[23−26]

Tetrathiafulvalene (TTF) is an electron donor[27] that has been employed in variety of molecular dyads and triads, including systems which involve a fullerene, porphyrin, or a perylenediimide as the electron acceptor.[28−34] Recently, a π-conjugated multiacceptor/donor array containing a TTF bridge between two fullerinecobalta-ene-1,2-dithiolate moieties, $[\{(C_{60}Ar_5)Co\}_2(S_2C_2S_2C{=}CS_2C_2S_2)]$, has been reported. Photoexcitation of this compound results in a charge separation between the TTF (donor) and the cobalt-ene-1,2-dithiolate (acceptor) constituents which relaxes via a resonance effect that extends throughout the acceptor components of the molecular array, including the fullerenes.[35] 6,7-Bis(methylthio)-tetrathiafulvalene ene-1,2-dithiolate ($TTF(SMe)_2$) has been used as an electron donor to $\{Ru(4,4'\text{-R-bpy})_2\}$ (R = H, CO_2Et or CO_2H) in a series of $[Ru(4,4'\text{-R-bpy})_2(TTF(SMe)_2)]$ dyes. Upon adsorption of the acid derivative onto TiO_2, a long-lived (20 ms) charge-separated state was observed,[23] a result which could have relevance for the development of dye-sensitized solar cells.[36]

Wright et al. showed that $[Fe_2(CO)_6\{$naphtha1ene-1,8-dithiolate$\}]$ complexes are robust proton-reduction catalysts, the redox potential of which can be tuned by varying the nature of the substituents on the napthalene.[37] Following this development, Samuel et al. bound naphthalene-4,5-*N*{(*p*-phenyl)-10,15,20-tri-*n*-pentylporphyrinzinc}monoimide-1,8-dithiolate to $\{Fe_2(CO)_6\}$ to form a compound in which a zinc porphyrin (a photosensitizer) is bridged by naphthalene monoimide (which can act as an electron relay) to a $\{Fe_2(\mu\text{-}S_2)(CO)_6\}$ unit (which catalyzes H_2 production from protons and electrons). Under 500−800 nm excitation, this dyad achieves light driven evolution of dihydrogen from a solution of trifluoroacetic acid by a mechanism that involves a charge separated [zinc porphyrin]$^+$-[naphthalene monoimide-$\{Fe_2S_2(CO)_6\}$]$^-$ excited state with the lifetime of 12 ps.[38]

$[Cp_2Mo($ene-1,2-dithiolate$)]$ compounds generally manifest a reversible one-electron oxidation[39−43] and can undergo a second one-electron oxidation to form the $[Cp_2Mo($ene-1,2-dithiolate$)]^{2+}$ dication.[44−46] The ease of oxidation and the absence of a readily accessible reduced (anionic) state make $[Cp_2Mo($ene-1,2-dithiolate$)]$ compounds attractive candidates for inclusion as the donor component in a donor−acceptor array. For example, the direct attachment of a $\{Cp_2Mo($ene-1,2-dithiolate$)\}$ center to a highly fluorescent 6-pterin results in a significant fluorescence quenching of the latter which is attributed to an efficient electron transfer within the dyad.[47] Despite these attractive redox properties, it appears that no $\{Cp_2Mo($ene-1,2-dithiolate$)\}$ moiety has been investigated as a synthon for photoinduced charge-separated systems.

The choice of acceptors for inclusion into donor−acceptor arrays is quite extensive with many of these being derived from a π-conjugated aromatic hydrocarbon and an aromatic acid diimides, e.g. perylene tetracarboxylic diimides (PTCDIs)[48−57] and naphthalene tetracarboxylic diimides (NDIs).[58−64] Thus, the strong electron accepting properties of these diimides, plus the characteristic spectroscopic profile of each redox state, has led to their extensive use as components in assemblies for photoinduced charge-separation.

Herein we report the synthesis of the first representative of a dithiolene-imide class of cascade electron transfer system. We

dx.doi.org/10.1021/ic301436t | *Inorg. Chem.* 2012, 51, 13181−13194

Table 1. Cyclic Voltammetric Data[a]

compound	1st reduction/V	2nd reduction/V	3rd reduction/V	1st oxidation/V	2nd oxidation/V
1[b]	−0.99 (0.09)	−1.43 (0.09)			
2	−0.97 (0.07)	−1.47 (0.07)	−2.16 (0.07)	−0.31 (0.07)	+0.35[c]
[Cp_2Mo(dt-Ph)]	−2.16 (0.07)			−0.33 (0.07)	+0.34[c]

[a]Potentials in V quoted to the nearest 0.01 V. Data reported at 0.1 V s^{-1} for 1 mM test solutions in DMF containing [$^nBu_4N$][BF_4] (0.2 M) as the supporting electrolyte. The anodic/cathodic peak separation ($\Delta E = E_p^a - E_p^c$) is given in brackets where applicable. ΔE for the Fc^+/Fc couple, used as the internal standard, was 0.07 V at 0.1 V s^{-1}. [b]In CH_2Cl_2 containing 0.2 M [$^nBu_4N$][BF_4] as the supporting electrolyte, limited solubility, ΔE for the Fc^+/Fc couple, used as the internal standard, was 0.08 V at 0.1 V s^{-1}. [c]Peak anodic potential (E_p^a).

have combined a {Cp_2Mo(ene-1,2-dithiolate)} metal center with an aromatic acid imide to form a donor-spacer-acceptor configuration; the highest occupied molecular orbital (HOMO) is located on the metal-ene-1,2-dithiolate (metalladithiolene), the lowest unoccupied molecular orbital (LUMO) is diimide-based, and these two functionalities are separated by a simple phenyl linker. We have shown that this system is capable of cascade electron transfer, leading to a spatially separated electron/hole pair with an appreciable lifetime, about 15 ns in CH_2Cl_2 at room temperature.

RESULTS AND DISCUSSION

Synthesis and Characterization. The new pro-ligand, **1**, was synthesized in four steps from *N*-(2-ethylhexyl)-1,4,5,8-naphthalene tetracarboxylic monoanhydride[65] (see Scheme 1 and Experimental Section). The first step involved condensation of the anhydride with 4-aminoacetophenone to produce the corresponding imide. Subsequent bromination, followed by reaction with potassium *O*-isopropylxanthate and treatment of the product with concentrated sulfuric acid yielded the dithiol-2-one, **1**.[66] Once isolated, this protected dithiolene is an intractable solid that, prior to hydrolysis and coordination to the metal center, necessitated pretreatment with concentrated sulfuric acid to achieve solubility followed by immediate extraction into CH_2Cl_2. Hydrolysis of a solution of the dithiol-2-one, **1**, in a mixture of CH_2Cl_2 and methanol with cesium hydroxide in the presence of [Cp_2MoCl_2] yields [Cp_2Mo(dt-Ph-NDI)] (**2**)(Scheme 1). This method appears versatile for the preparation of [Cp_2Mo(dt-Ph-R)] (R = imide) compounds as demonstrated by the synthesis of [Cp_2Mo(dt-Ph-NI)] (NI = naphthalene dicarboxylic monoimide) (Scheme 1, see Supporting Information for synthesis and characterization).

Cyclic Voltammetry. **1** is insoluble in dimethylformamide (DMF) but sparingly soluble in CH_2Cl_2; therefore cyclic voltammetric data for **1** were collected for a CH_2Cl_2 solution containing [$^nBu_4N$][BF_4] (0.2 M). A cyclic voltammetric study of **2** was performed for this compound dissolved in DMF containing [$^nBu_4N$][BF_4] (0.2 M) (Table 1 and Figure 1) and showed three reversible, one-electron reduction processes at $E_{1/2}$ of −0.97, −1.47, and −2.16 V vs Fc^+/Fc and a reversible, one-electron oxidation process at −0.31 V vs Fc^+/Fc. In addition, an oxidation peak, at E_p^a +0.35 V vs Fc^+/Fc, was observed but was not studied further. Electron paramagnetic resonance (EPR) and UV/vis spectroscopic studies (vide infra) showed that the first and second reductions are NDI based.[62,63] Consistent with this, each of these processes occurs at a potential similar to that for the corresponding process of **1** (Table 1). Each of the two oxidations and the third reduction occurs at a potential very close to that reported for [Cp_2Mo(dt-Ph)] ($E_{1/2}$: −0.33, +0.34 and −2.16 V, respectively)[43] and are assigned to the corresponding redox process of the metalladithiolene moiety of **2**.

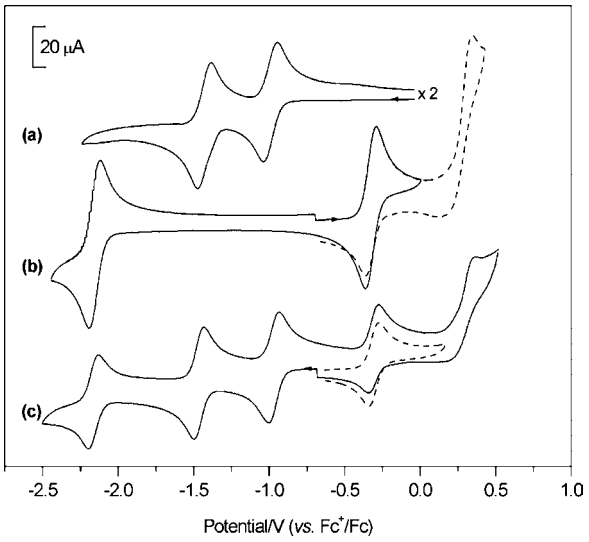

Figure 1. Cyclic voltammetric information recorded for (a) **1** in CH_2Cl_2, (b) [Cp_2Mo(dt-Ph)], and (c) **2** in dmf; each solution contained [$^nBu_4N$][BF_4] (0.2 M) and the data were recorded at an ambient temperature and a 0.1 V s^{-1} scan rate.

These cyclic voltammetric data indicate that for **2** the HOMO is metalladithiolene based and the LUMO is NDI-based; therefore, consistent with our molecular design, the lowest excited state(s) in **2** should be of a charge-separated nature. Our picosecond time-resolved IR and ultrafast transient absorption (TA) studies (vide infra) demonstrate the realization of this concept. Also, the nature of the frontier orbitals has been probed further by UV/vis, IR and EPR spectroscopic investigations and density functional theory (DFT) calculations.

UV/vis Spectroscopy. The electronic absorption spectrum of **2** is shown in Figure 2, and details of the principal features are summarized in Table 2. The broad, relatively weak absorption centered at 534 nm corresponds to that in the region 490−570 nm observed for [Cp_2Mo(SC(R)C(R′)S)] (R = H, CH_3 or Ph; R′ = Ph, pyridine, pyrene or quinoxaline) in CH_2Cl_2 which Hsu et al.[42] assigned to a 1,2-enedithiolate→Mo ligand to metal charge transfer (LMCT) transition. Also, these authors considered that the absorption of these compounds in the region 320−380 nm arises from an intraligand charge transfer transition (ILCT), the donor orbital being located on the ene-1,2-dithiolate and a π^* orbital of the aromatic R′ group being the acceptor. The UV/vis spectrum of [Cp_2Mo(dt-Ph)][43] (see inset of Figure 2) is analogous to that of the [Cp_2Mo(SC(R)C(R′)S)] compounds. Thus, [Cp_2Mo(dt-Ph)] and **2** both manifest a weak absorption at about 420 nm that, based on studies reported for [Cp_2MoS_2],[67] we assign to a sulfur→Mo transition (LMCT). Transitions in the higher energy region of the UV/vis spectrum of **2**, notably two sharp

dx.doi.org/10.1021/ic301436t | Inorg. Chem. 2012, 51, 13181−13194

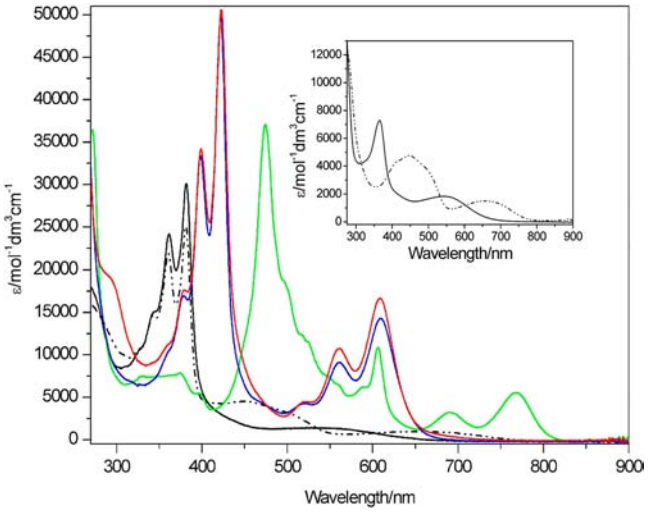

Figure 2. UV−vis spectra of neutral **2** (black solid line), $[\mathbf{2}]^{+}$ (dotted-dashed line), $[\mathbf{2}]^{-}$ (green solid line), $[\mathbf{2}]^{2-}$ (blue solid line) and $[\mathbf{2}]^{3-}$ (red solid line). Inset: UV−vis spectrum of $[Cp_2Mo(dt\text{-}Ph)]$ (solid line) and $[Cp_2Mo(dt\text{-}Ph)]^{+}$ (dotted-dashed line). All spectra were recorded in DMF containing $[^{n}Bu_4N][BF_4]$ (0.2 M) at 273 K using an OTE.

Table 2. Principal Features of the Electronic Absorption Spectra of $[\mathbf{2}]^{n}$ (n = 1+, 0, 1−, 2−, and 3−) and $[Cp_2Mo(dt\text{-}Ph)]^{n}$ (n = 0, 1+, or 1−) in DMF Containing $[^{n}Bu_4N][BF_4]$ (0.2 M) as a Supporting Electrolyte[a]

compound	λ_{max}/nm ($\varepsilon \times 10^{-4}$/mol^{-1} dm^3 cm^{-1})
$[\mathbf{2}]^{0}$	361 (2.4), 382 (3.0), 534 (0.1)
$[\mathbf{2}]^{+}$	327 (1.1), 343 (1.5), 361 (2.2), 381 (2.5), 448 (0.5), 645 (0.1)
$[\mathbf{2}]^{-}$	374 (0.8), 474 (3.7), 606 (1.1), 690 (0.3), 768 (0.6)
$[\mathbf{2}]^{2-}$	379 (1.7), 399 (3.3), 422 (5.0), 518 (0.4), 561 (0.9), 610 (1.4)
$[\mathbf{2}]^{3-}$	379 (1.8), 399 (3.4), 423 (5.1), 522 (0.4), 560 (1.1), 608 (1.7)
$[Cp_2Mo(dt\text{-}Ph)]^{0}$	364 (0.7), 547 (0.2)
$[Cp_2Mo(dt\text{-}Ph)]^{+}$	418 (0.4), 447 (0.5), 484 (0.4), 657 (0.2)
$[Cp_2Mo(dt\text{-}Ph)]^{-}$	291 (1.9), 349 (0.9), 424 (0.4), 571 (0.3)

[a]The spectra were recorded at 273 K using an OTE.

bands at 382 and 361 nm are assigned to intra-NDI absorptions[59,62,63] which probably obscure the ene-1,2-dithiolate→Ph π^* based ILCT transition.

We augmented the CV studies of **2** by undertaking UV/vis spectroelectrochemical investigations for this compound at 273 K in DMF solution containing $[^{n}Bu_4N][BF_4]$ (0.2 M) as the supporting electrolyte. The absorption spectra recorded are shown in Figure 2; the principal absorptions observed are summarized in Table 2 together with the corresponding data for $[Cp_2Mo(dt\text{-}Ph)]^{n}$ (n = 0, 1+ or 1−);[43] also, the UV/vis spectrum of $[Cp_2Mo(dt\text{-}Ph)]^{+}$ is shown in the inset of Figure 2. Under the conditions of these experiments, each of the redox processes studied was chemically reversible.

Oxidation of **2** to $[\mathbf{2}]^{+}$ did not lead to any significant change in the profile of the higher energy region of the UV/vis spectrum. However, at lower energies, the 534 nm band disappeared, and new bands at 448 and 645 nm appeared, changes which correspond closely to those observed for the one-electron oxidation of $[Cp_2Mo(dt\text{-}Ph)]$[43] (see Figure 2 inset). Reduction of **2** to $[\mathbf{2}]^{-}$ led to a UV/vis spectrum with a significantly different profile, consistent with the formation of an NDI radical anion.[62,68] Reduction to $[\mathbf{2}]^{2-}$ produced a spectrum, the UV region of which was characteristic of $[NDI]^{2-}$.[62,68] Reduction to $[\mathbf{2}]^{3-}$ led to a small increase in the intensity of these absorptions, but the minimal perturbation of these band positions suggests that this reduction is localized on the ene-1,2-dithiolene moiety.

EPR Spectroscopy. One-electron oxidation of **2** in DMF produced a green/brown solution of $[\mathbf{2}]^{+}$, the fluid solution EPR spectrum of which displayed an isotropic signal with g_{iso} of 2.012. This spectrum (Figure 3) showed hyperfine splitting due

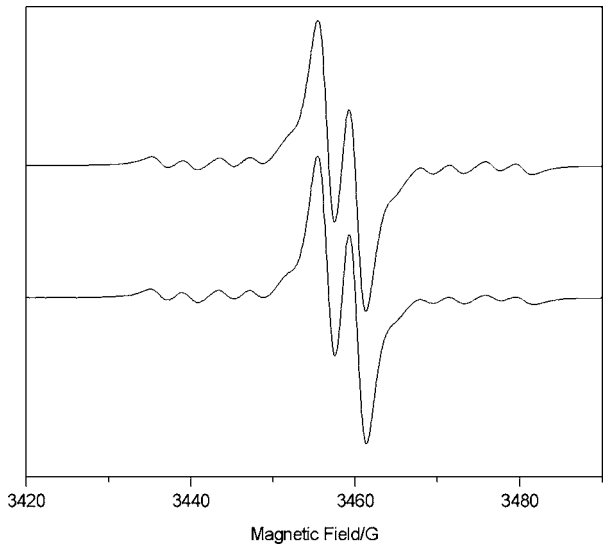

Figure 3. Lower trace: EPR spectrum of $[\mathbf{2}]^{+}$ (1 mM) in DMF containing $[^{n}Bu_4N][BF_4]$ (0.2 M) at 298 K. Upper trace: simulated spectrum with g_{iso} = 2.012, A_{Mo} 7.61 × 10^{-4} and a_H 3.38 × 10^{-4} cm^{-1} created using a Lorentzian line shape and a 2.3 G line width.

to coupling of the unpaired electron with the molybdenum center (^{95,97}Mo: 25.5%, I = 5/2) and a single hydrogen atom, presumably that of the ene-1,2-dithiolate group. On cooling this solution to 77 K, a rhombic EPR spectrum was observed with g_1 2.030, g_2 2.014 and g_3 1.996, but no distinct hyperfine coupling to either the metal center or the hydrogen atom was observed at this temperature (Supporting Information, Figure SI5). Results obtained from both fluid and frozen solution EPR measurements are very similar to the corresponding data obtained for $[Cp_2Mo(dt\text{-}Ph)]^{+}$[43] and are consistent with the HOMO of **2** being based on the metalladithiolene moiety.

One-electron reduction of **2** in DMF produced a purple/red solution of $[\mathbf{2}]^{-}$, the fluid solution EPR spectrum of which comprised an isotropic signal with g_{iso} 2.004 which manifest hyperfine coupling of the unpaired electron to six hydrogen nuclei and two nitrogen nuclei (Figure 4). This EPR spectral profile for $[\mathbf{2}]^{-}$ and the simulated hyperfine coupling parameters are consistent with the formation of an NDI based radical-anion; therefore, we conclude that the LUMO of $[Cp_2Mo(dt\text{-}Ph\text{-}NDI)]^{-}$ is localized on the NDI moiety.[62,63,68]

One-electron reduction of $[\mathbf{2}]^{-}$ yielded a green solution of $[\mathbf{2}]^{2-}$, the fluid solution EPR spectrum of which was essentially identical to that of $[\mathbf{2}]^{-}$ albeit significantly weaker and double integration of this spectrum gave an intensity about 10% that of $[\mathbf{2}]^{-}$. These data are taken to indicate that the second reduction of **2**, like the first, is NDI-based and results in a spin-paired diamagnetic species. [Results from UV/vis spectroelectrochem-

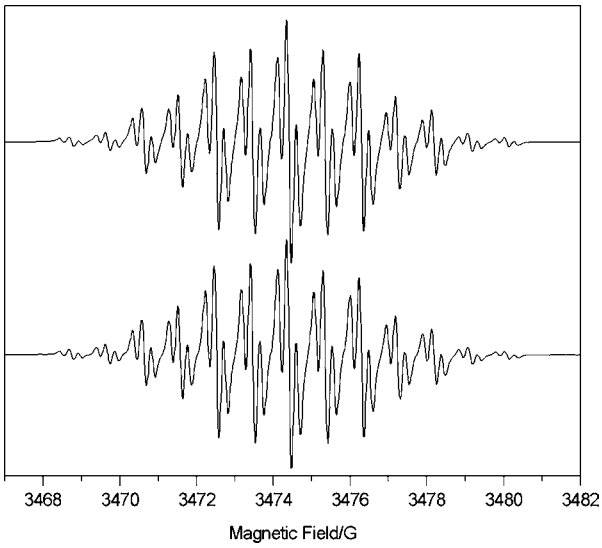

Figure 4. Lower trace: EPR spectrum of $[\mathbf{2}]^-$ (1 mM) in DMF containing $[^n Bu_4N][BF_4]$ (0.2 M) at 298 K. Upper trace: simulated spectrum with g_{iso} = 2.004, a_{4H} 1.77 × 10^{-4}, a_{2H} 0.22 × 10^{-4}, and a_{2N} 0.89 × 10^{-4} cm^{-1} created using a Lorentzian line shape and a 2.3 G line width.

istry suggested that the third reduction of **2**, at −2.16 V vs Fc^+/Fc, was chemically reversible. Hence, the controlled potential electrolysis to reduce $[\mathbf{2}]^{2-}$ was attempted and yielded a green solution of $[\mathbf{2}]^{3-}$. The fluid solution EPR spectrum of $[\mathbf{2}]^{3-}$ was very weak; however, on cooling the solution to 77 K a spectrum consisting of two distinct features centered around *g* 1.912 and 2.004 was obtained (Supporting Information, Figure SI6); it was unclear whether these features were derived from a single species or a mixture of products and analysis of these data was not taken further.]

FTIR Spectroscopy. The FTIR spectra of **2**, $[\mathbf{2}]^+$, and $[\mathbf{2}]^-$ are presented in Figure 5. The FTIR spectrum of **2** in the range 1500−1800 cm^{-1} is dominated by absorptions from the NDI moiety ($\upsilon_{(C=O)}$ 1717(sh), 1708, 1678(sh), 1669; $\upsilon_{(C=C\text{-}NDI)}$, naphthalimide core breathing, 1582 cm^{-1}) which correlate well with those reported for the asymmetrically substituted $[Pt(phen\text{-}NDI)Cl_2]$ ($\upsilon_{(C=O)}$ 1723(sh), 1705, 1688(sh), 1670; $\upsilon_{(C=C\text{-}NDI)}$ 1583 cm^{-1}),[62] including the splitting of the carbonyl bands. Oxidation of **2** to $[\mathbf{2}]^+$ does not significantly change the profile of the major bands assigned to the NDI moiety (i.e., $[\mathbf{2}]^+$ has $\upsilon_{(C=O)}$ 1708, 1669; $\upsilon_{(C=C\text{-}NDI)}$ 1582 cm^{-1}); the similarity between IR bands for **2** and $[\mathbf{2}]^+$ provides further evidence for this oxidation involving the loss of an electron from an orbital that is not NDI-based. The absorption at 1529 cm^{-1} in **2** is assigned to the C═C stretching of the ene-1,2-dithiolate moiety ($\upsilon_{(C=C\text{-}DT)}$), consistent with results reported previously for other coordinated ene-1,2-dithiolates.[69−71] The shift in this band to 1507 cm^{-1} in $[\mathbf{2}]^+$ is consistent with the results of the DFT calculations for **2** (vide infra) which indicate that the HOMO is ene-1,2-dithiolate based.

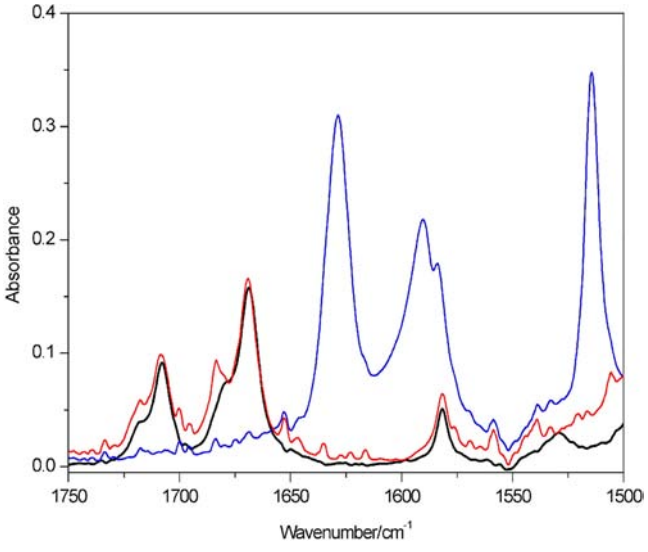

Figure 5. FTIR spectra of **2** (black), $[\mathbf{2}]^-$ (blue), and $[\mathbf{2}]^+$ (red) recorded in CH_2Cl_2 (ca. 1 mM) containing $[^n Bu_4N][BF_4]$ (0.4 M) at room temperature.

Reduction of **2** to $[\mathbf{2}]^-$ results in a significant shift of the $\upsilon_{(C=O)}$ bands to lower frequencies (1629, 1590, 1514 cm^{-1}; Figure 5). These changes correspond to a decrease in the C═O bond order resulting from the population of a π^* orbital, consistent with the results of the DFT calculations for **2**, which indicate that the LUMO is NDI-based, and the IR bands observed for $[Pt(phen\text{-}NDI)Cl_2]^-$ ($\upsilon_{(C=O)}$ 1629, 1592, 1514 cm^{-1}).[62] The band assigned as $\upsilon_{(C=C\text{-}NDI)}$ in **2** is essentially unperturbed upon reduction (being at 1584 cm^{-1} in $[\mathbf{2}]^-$).

DFT calculations. To gain further insight into the electronic structure of **2** we have performed a gas phase density functional (DFT) geometry optimization of a model of **2** in which the 2-(ethyl)-hexyl group pendant to the NDI unit in **2** was replaced by a methyl group. These calculations generated a structure where the geometry within the {MSCCS} metallacycle is similar to that found previously for $[Cp_2Mo(dt\text{-}Ph)]$[43] (Supporting Information, Table SI2) and in which the dihedral angles between the {MoSCCS} metallacycle and the planes of the Ph and NDI rings are 31.3° and 61.9°, respectively. Thus, the inclusion of a NDI unit pendant to the Ph ring of $[Cp_2Mo(dt\text{-}Ph)]$ does not appear to significantly modify the geometry of the {MoSCCS} metallacycle core.

The manifold of the frontier orbitals possessing {MoSCCS} metallacycle character in this model of **2** (Table 3, Figure 6) is very similar to that found previously for gas phase calculations accomplished for $[Cp_2Mo(dt\text{-}Ph)]$.[43] Thus, the HOMO (170a) is primarily (65.7%) ene-1,2-dithiolate π_3 in character, i.e., C−C π-bonding and C−S π-antibonding. A series of unoccupied orbitals localized primarily on the NDI moiety (notably 171a, 173a, 175a, and 176a) are interspersed between the $\{Cp_2MoSCCS\}$-based antibonding orbitals (172a, 174a, 177a, and 178a) and above the ene-1,2-dithiolate π_3-based HOMO (170a).

The energies of the HOMO and LUMO (Table 3) calculated for **2** in the gas phase are very similar (within 0.008 eV) and appear to be inconsistent with the difference in potentials (0.66 V) for the first oxidation and reduction processes measured for **2** in dmf (0.2 M $[^n Bu_4N][BF_4]$) solution (Table 1, Figure 1). The form and relative ordering of the frontier orbitals calculated for **2** are consistent with the information obtained from the UV/vis, IR, and EPR studies of **2**, $[\mathbf{2}]^+$, and $[\mathbf{2}]^-$ (vide ultra) and indicate that the HOMO of this molecule is metalladithiolene-based and the LUMO is NDI-based. The information presented in Table 3 and Figure 6 show that these two regions of the molecule are electronically distinct with only one orbital (167a) involving significant contributions from both components. This latter point is corroborated by our

dx.doi.org/10.1021/ic301436t | *Inorg. Chem.* 2012, 51, 13181−13194

Table 3. Nature, Energy, and Composition of the Frontier Orbitals Obtained from DFT Calculations for a Model of 2

orbital				composition /%				
designation		nature	energy/eV	Cp_2	Mo	S_2C_2	Ph	NDI
179a	L+8	Mo $d_{x^2-y^2}$ + d_{xy} + S_2C_2 σ_1 + Ph	−1.501	6.0	8.5	25.2	50.3	10.0
178a	L+7	Mo $d_{x^2-y^2}$ + d_{z^2} + Cp_2 + S_2C_2 σ_1	−1.627	27.3	53.5	14.9	3.6	0.8
177a	L+6	Mo d_{xz} + Cp_2 + S_2C_2 σ_2	−1.851	33.6	36.4	25.6	3.8	0.6
176a	L+5	NDI	−2.124	0.0	0.1	0.0	0.1	99.8
175a	L+4	NDI	−2.182	0.9	1.2	0.1	0.0	97.7
174a	L+3	Mo d_{xy} + Cp_2	−2.208	38.4	47.9	6.6	3.4	3.6
173a	L+2	NDI	−2.654	0.4	0.6	1.4	3.7	93.9
172a	L+1	Mo d_{yz} + S_2C_2 π_3 + Cp_2	−2.884	29.4	51.7	17.0	1.0	0.9
171a	LUMO	NDI	−4.156	0.4	0.1	1.3	0.2	98.0
170a	HOMO	S_2C_2 π_3 + Mo Cp_2	−4.164	18.6	5.8	65.7	7.3	2.7
169a	H-1	Mo $d_{x^2-y^2}$ + d_{z^2}	−4.595	11.7	76.9	10.6	0.8	0.0
168a	H-2	S_2C_2 π_2 + Ph	−5.505	10.3	2.0	58.1	25.9	3.7
167a	H-3	Ph + S_2C_2 π_2	−6.043	12.8	4.7	45.5	25.0	12.0
166a	H-4	Ph + S_2C_2 σ_2	−6.098	7.6	3.0	22.6	57.2	9.5
165a	H-5	S_2C_2 σ_2 + Mo d_{xz}	−6.204	11.9	3.9	35.0	40.1	9.1
164a	H-6	NDI	−6.345	2.8	0.7	4.6	5.0	86.8

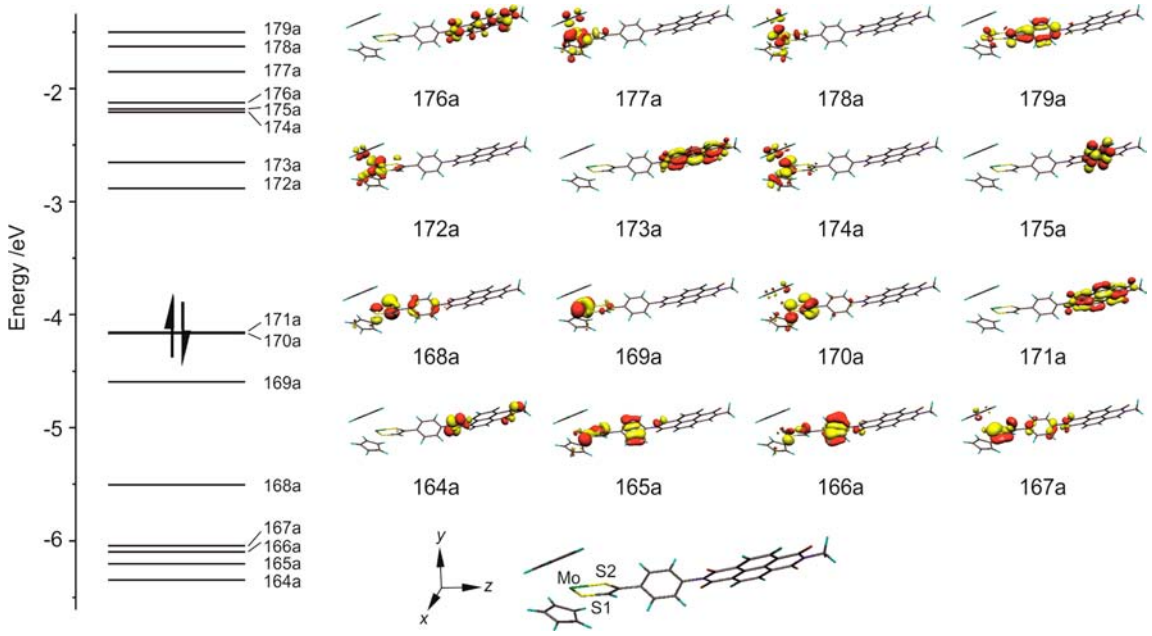

Figure 6. Energy level diagram and pictorial representations of the Kohn−Sham frontier orbitals of the gas phase geometry optimized structure of [Cp_2Mo(dt-Ph-NDI)].

observation of the lack of an electronic transition that we could assign to a HOMO to LUMO transition. This results from the poor orbital overlap between the spatially separated metal-ladithiolene and NDI-based HOMO and LUMO, respectively.

Picosecond Time-Resolved IR Studies. Time-resolved infrared spectroscopy (TRIR) was used to probe the nature and dynamics of the excited state of **2** in CH_2Cl_2 solution (ca. 1 mM) following excitation by a 400 nm ∼120 fs laser pulse. The TRIR data recorded from 1300 to 1750 cm^{-1} are presented in Figure 7.

The 400 nm excitation led to an instant depletion of the ground state IR bands localized on both the NDI and ene-1,2-dithiolate moieties, the most pronounced bleaches being those of NDI $\nu_{(C=O)}$ at 1721/1711 cm^{-1} (A in Figure 7) and 1673/1682 cm^{-1} (C), $\nu_{(C=C\text{-}NDI)}$ of the naphthalene-part of NDI at 1582 cm^{-1} (G), $\nu_{(C=C\text{-}DT)}$ at 1531 cm^{-1} (H),[69−71] and the NDI-localized bands at 1494, 1453, 1372, and 1345 cm^{-1}. The instant appearance of new transient bands was also observed at 1701 cm^{-1} (B), 1663 cm^{-1} (D), 1629 cm^{-1} (E), about 1578 and 1591 cm^{-1} (F) (or one broad band, punctured by a narrow ground state bleach at 1582 cm^{-1} (G)), 1511 cm^{-1} (I), 1482, 1446, 1363, and 1334 cm^{-1}.

Up to about 100 ps after the 400 nm excitation, the evolution of the TRIR spectrum was complicated (Figure 7). The spectral dynamics and the spectral profile were analyzed by performing a global fit to the data. This procedure revealed that a minimum of three components are sufficient to describe the majority of the features developed in the TRIR spectrum; these components possess lifetimes of 1.88(±0.11) ps, 22(±1) ps and >10 ns; the last encompasses those spectral features with a lifetime considerably greater than the time scale of the experiment. Notably, the features at 1629 (E), 1591 (F), and 1514 cm^{-1} (the latter overlaps with the $\nu_{(C=C\text{-}DT)}$ 1511 cm^{-1} (I) band) which correspond to bands in the IR spectrum of

dx.doi.org/10.1021/ic301436t | Inorg. Chem. 2012, 51, 13181−13194

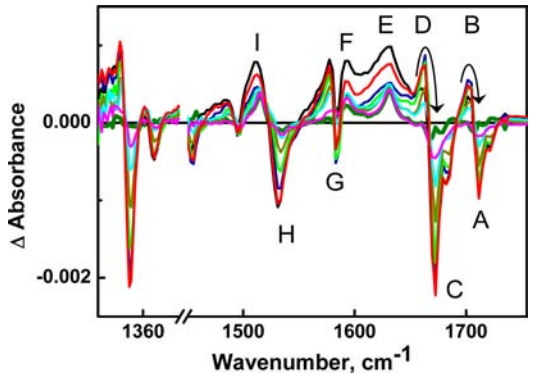

Figure 7. Time-resolved IR spectra of a solution of **2** in CH_2Cl_2 (ca. 1 mM) obtained at a series of time delays following excitation by a 400 nm ~120 fs laser pulse: 1.5 ps (black solid line), 2.5 ps (red solid line), 5 (dark blue solid line), 10 (green solid line), 20 (mustard solid line), 30 (turqoise solid line), 50 (magenta solid line) and 1000 (dark green solid line) ps after the laser pulse. Kinetic traces at the labeled frequencies are shown in Figure 8.

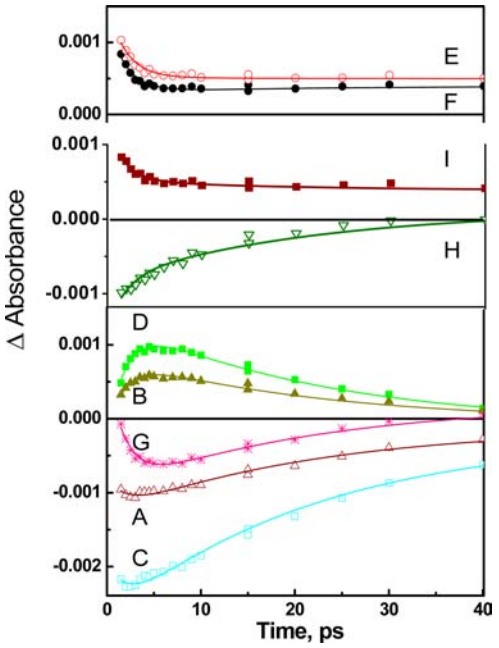

Figure 8. Decay traces obtained in the TRIR for a solution of **2** in CH_2Cl_2 (ca. 1 mM) following excitation with a 400 nm ~120 fs laser pulse. The solid lines were obtained by a global fit analysis of the experimental data, which are represented by the markers, on the basis of three transient species with lifetimes of τ_1 = 1.88(±0.11) ps, and τ_2 = 22.2(±1.0) ps plus a constant (τ > 10 ns). The labels A–I on the panels correspond to the band positions indicated in Figure 7.

NDI^- and $[\mathbf{2}]^-$, appeared instantly in the TRIR spectrum (Figure 7), indicating that the NDI^- anion is present in the first excited state detected in TRIR experiments, which has the 1.88 ps lifetime.

Immediately after the laser pulse, the IR bands between 1550 and 1650 cm^{-1} (E and F) were rather broad, indicating the presence of one or more vibrationally hot states. The evolution of the initial TRIR spectrum with the 1.88 ps lifetime was accompanied by a partial decay of the broad features between 1550 and 1650 cm^{-1} (E and F) and a notable increase in the intensity of the NDI-based transient bands at 1701 (B) and 1663 (D) cm^{-1} which correspond to the parent bleaches of **2** at 1711 (A) and 1673 (C) cm^{-1}, respectively.

The transient bands at 1701 (B) and 1663 cm^{-1} (D) are assigned to the vibrationally hot electronic ground state of the molecule, likely due to the $\nu_1 \rightarrow \nu_2$ transition with a typical anharmonic shift with respect to the $\nu_0 \rightarrow \nu_1$ transition. The kinetic process with the 22 ps lifetime corresponds to the decay of these NDI-based bands and the concomitant recovery of the ground state bleaches A, C, G, and H. This decay is attributed to the cooling of the vibrationally hot electronic ground state. This lifetime (22 ps) is very similar to the one (19 ps) reported previously for the corresponding cooling process of the NDI fragment in $[Pt(phen\text{-}NDI)Cl_2]$.[62]

The NDI^- anion bands at 1629 (E) and 1591 cm^{-1} (F) also exhibit a considerable narrowing with the about 22 ps lifetime which could be attributed to the cooling of the vibrationally hot excited state. Formation of the vibrationally hot electronic states[72] arises since the decay of the first electronic excited state releases a large amount of energy within a few picoseconds; thus, decay to the ground state would release about 3.1 eV (as estimated from the energy of the excitation light of 400 nm) and decay to $[Cp_2\{Mo(dt)\}^+\text{-}Ph\text{-}\{NDI^-\}]^*$ would release about 2.5 eV (as estimated from the difference between the redox potentials for the formation of $[\mathbf{2}]^+$ and $[\mathbf{2}]^-$ (vide ultra)).

Thus, the fast (1.88 ps) component corresponds to the lifetime of the first excited state detected by the TRIR experiments, which contains the NDI^- anion; this excited state decays to the ground state and to a different excited state which also contains the NDI^- anion. The second component (lifetime 22 ps) observed in the TRIR data corresponds to various cooling processes of vibrationally hot states.

The evolution of the TRIR spectrum was complete by about 100–150 ps after the laser pulse and the final spectral profile, corresponding to that of the 1000 ps delay, is shown in Figure 7 (dark green line). The major transient bands in the TRIR spectra of the final excited state (Figure 9) correspond to those

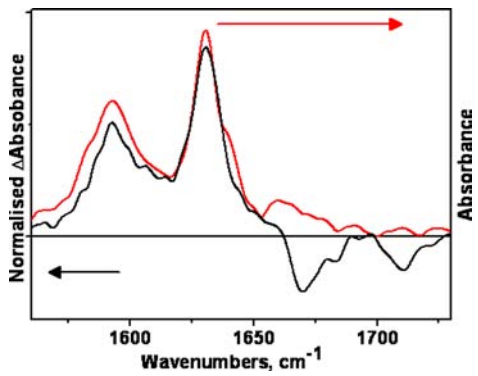

Figure 9. Comparison between the time-resolved IR spectrum of **2** recorded 1000 ps after excitation with a 400-nm ~120 fs laser pulse (black solid line) and the IR spectrum of electrochemically generated $[\mathbf{2}]^-$ (red solid line).

of the NDI^- anion (at 1629, 1590, and 1514 cm^{-1}). The relative intensities of these transients and the corresponding ground state bleaches at 1711 and 1673 cm^{-1} are consistent with the IR data for $[\mathbf{2}]^-$ (Figure 5), confirming that the only NDI-related transient contains the NDI^- anion (Figure 9).

Furthermore, in addition to the bleaches of the $\upsilon_{(C=O\text{-}NDI)}$ bands of the ground state of **2** at 1711 and 1673 cm^{-1},

dx.doi.org/10.1021/ic301436t | Inorg. Chem. 2012, 51, 13181–13194

bleaching of the ($\upsilon_{(C=C\text{-}DT)}$) band at 1531 cm^{-1} was also observed, indicating a perturbation of the metalladithiolene moiety in the final excited state. The IR bands of $[\mathbf{2}]^+$ (Figure 5) are weak in comparison to those of the NDI^- anion and generally overlap in energy. Therefore, no prominent transient features in the TRIR spectrum can be attributed to $[\mathbf{2}]^+$ although it could be responsible for the weak shoulder at about 1660 cm^{-1}, where no IR absorbances of the NDI^- anion are anticipated. The TRIR spectrum remained constant up to an equipment-limited time delay of 2 ns and the lifetime of this charge-separated state was determined by nanosecond flash photolysis (vide infra).

To interpret the TRIR data it is necessary to consider the nature of the excited states potentially formed upon 400 nm excitation. Given the assignments of the UV/vis spectrum of **2** (Figure 2), two possibilities exist: (i) population of an NDI excited state or (ii) population of lower-lying metalladithiolene-based excited states derived from the ene-1,2-dithiolate→Mo and sulfur→Mo LMCT transitions at about 534 and 420 nm, respectively. On the basis of the extinction coefficients at 400 nm of **2** (5990 M^{-1} cm^{-1}) and of $[Cp_2Mo(dt\text{-}Ph)]$ (2400 M^{-1} cm^{-1}), the ratio between these two pathways can be estimated as 3:2, which indicates a significant contribution of NDI-based transitions in the absorption of light at 400 nm.

The LMCT transitions are unlikely to lead to a charge-separated state which involves the NDI^- anion, as they are accompanied by a shift of electron density away from the NDI moiety. The information obtained from the TA experiments (vide infra) at a different excitation wavelength (383 nm) indicates that the charge-separation process leading to the final $[Cp_2\{Mo(dt)\}^+\text{-}Ph\text{-}\{NDI^-\}]^*$ state does stem from an $^1NDI^*$ excited state.

The LMCT states populated by 400 nm excitation are likely to decay to the ground state via ultrafast nonradiative processes, producing a vibrationally hot ground state. The instant appearance in the TRIR spectrum of the bleach of the $\upsilon_0 \rightarrow \upsilon_1$ vibrational transition of the $\nu_{(C=C\text{-}DT)}$ band of the dithiolene moiety at 1531 cm^{-1} (H) (Figure 7) and the appearance of the corresponding $\upsilon_1 \rightarrow \upsilon_2$ transition of the vibrationally hot electronic ground state at a lower energy (1511 cm^{-1} (I)) with an anharmonic shift of about 20 cm^{-1} is consistent with this postulate, as is the fact that the dynamics of 1531/1511 cm^{-1} bands differ from those of the other bands in the TRIR spectrum. Since the 1511 cm^{-1} (I) transient band overlaps with an absorption of the NDI^- anion it is difficult to extract accurate dynamic information; however, the *partial* recovery of the $\nu_{(C=C\text{-}DT)}$ bleach at 1531 cm^{-1} (H) occurs with a 11(±1) ps lifetime. We attribute this value to vibrational relaxation of the hot ground state; the observed lifetime is similar to the one reported previously for vibrational relaxation of $\nu_{(C\equiv C)}$ in Pt(II) acetylides.[73]

Thus, the information obtained from these TRIR studies is consistent with the formation of a charge-separated state of **2** which is largely {Mo/dithiolene-to-NDI} in character, i.e., $[Cp_2\{Mo(dt)\}^+\text{-}Ph\text{-}\{NDI^-\}]^*$.

Ultrafast TA Studies. The dynamics of excited state(s) of **2** were investigated by TA spectroscopy using a 383 nm ~120 fs laser pulse. This excitation energy is essentially coincident with the absorption maximum of the intra-NDI transition at 382 nm and may also excite the ene-1,2-dithiolate→Ph π^* ILCT transition at about 365 nm (vide ultra). It is noted that the extinction coefficient of $[Cp_2Mo(dt\text{-}Ph)]$ at 383 nm is about 4000 M^{-1} cm^{-1},[43] significantly less than that of about 29,000 M^{-1} cm^{-1} for the intra-NDI transition; therefore, the photophysics under 383 nm excitation should originate primarily from the initial population of the $^1NDI^*$ state. The excitation resulted in the instantaneous appearance of new absorptions in the visible region; the spectral changes were monitored from 420 to 760 nm (Figure 10).

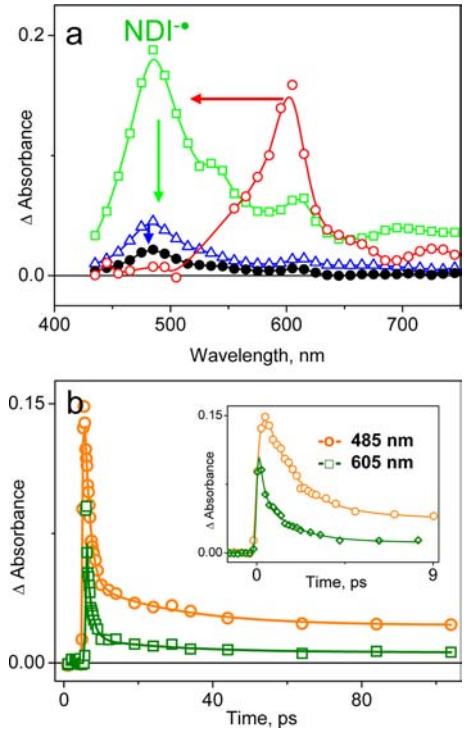

Figure 10. (**a**) Reconstructed TA spectra of different excited states of **2** in CH_2Cl_2, obtained subsequent to the initial excitation by a 383 nm ~120 fs laser pulse. First excited state (A), red open circles; second excited state (B), green open squares; third excited state (C), blue open triangles; final excited state (D), black solid circles. These spectra were constructed from the experimental data using a global fit analysis and an A→B→C→D model with the lifetimes of 0.2(±0.1), 1.47(±0.2), and 24(±2) ps. The lifetime for the state D could not be determined on the time scale of this experiment. (**b**) Kinetic traces at 605 and 485 nm (markers are experimental data; the solid line is a fit produced using parameters obtained from the global fit, see text for details).

On the picosecond time scale, the evolution of the visible spectrum was consistent with the formation of several excited states. The spectra shown in Figure 10a were obtained from the transient spectra by a global fit procedure (simultaneous exponential analysis) of the decay traces integrated over a 10-nm spectral interval across the 420 to 760 nm spectral range (see Experimental Section). A minimum of three mono-exponential decay components with lifetimes of 0.2(±0.1), 1.47(±0.2), and 24(±2) ps plus one long-lived component which was modeled as a constant on the time scale of the experiment (up to 1.6 ns) were sufficient to fit the kinetic data (Figure 10b). Therefore, each kinetic trace was fitted with a tri-exponential decay and a constant term, all convolved with the instrument response function. The initial spectrum shows a well-defined absorption maximum at 605 nm and shoulders at about 655 and 725 nm which is analogous to that observed for a local $^1NDI^*$ excited state in the symmetric *N,N′*-di-isooctyl-NDI molecule.[74a] This first excited state (A) evolves with the

dx.doi.org/10.1021/ic301436t | *Inorg. Chem.* 2012, 51, 13181−13194

lifetime of 0.2(±0.07) ps into the second excited state (B), the spectrum of which is characteristic of the NDI-radical anion[59,68,75,76] with absorptions at 485 and 609 nm and shoulders at 534 and 692 nm (Figure 2). The spectrum then decreased significantly in intensity with a lifetime of 1.47(±0.03) ps to produce the spectrum of the third excited state (C); this state decayed with a lifetime of 24(±2) ps to produce the final spectrum of D which persisted on the time-scale of the experiment, up to 2 ns.

Thus, analogous to the TRIR experiments, the evolution of the transient spectrum is complete within 100 ps (Figure 10b) to yield state D, the visible spectrum of which corresponds to that of NDI^- (Figure 11). (NB. The very small increase in the optical density in the spectrum of the transient species at about 500 nm and about 670 nm compared to that of $[\mathbf{2}]^-$ is attributed to the presence of the $\{metalladithiolene\}^+$ moiety).[43] Thus, the 383 nm ~120 fs excitation effects the formation of the $[Cp_2\{Mo(dt)\}^+\text{-Ph-}\{NDI^-\}]^*$ charge-separated state.

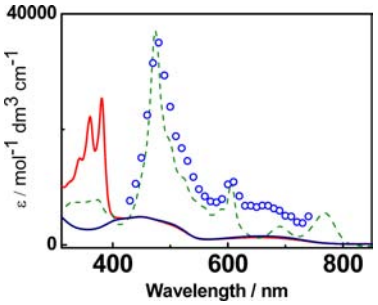

Figure 11. Comparison of the UV/vis absorption spectrum of D, the third excited state of **2** (blue open circles) and electrochemically generated $[\mathbf{2}]^-$ (green dashed line), $[\mathbf{2}]^+$ (red solid line), and $[Cp_2Mo(dt\text{-}Ph)]^+$ (blue solid line).

The dynamics of the excited state of **2** obtained from the TA experiments are consistent with those obtained from the TRIR investigations. The ultrafast component with the lifetime about 0.2 ps, which cannot be resolved in TRIR, evolves into the spectrum of the vibrationally hot local charge-transfer state $[Cp_2\{Mo(dt)\}\text{-}Ph^+\text{-}\{NDI^-\}]^*$. The other two dynamic components observed in the TA study (1.47(±0.03) and 24(±2) ps) are in good agreement with those determined from the TRIR investigation (1.88(±0.11) and 22(±1) ps). The former is attributed to the decay of the first charge-transfer state to the ground state (leading to formation of the vibrationally hot ground state), and to the vibrationally hot final charge-separated state, $[Cp_2\{Mo(dt)\}^+\text{-Ph-}\{NDI^-\}]^*$. The 22(±1) ps component is considered to involve cooling of vibrationally hot ground *and* charge-separated states leading to the formation of the final, vibrationally relaxed charge-separated state, $[Cp_2\{Mo(dt)\}^+\text{-Ph-}\{NDI^-\}]^*$.

Nanosecond TA Spectroscopy. Since the charge separated state, $[Cp_2\{Mo(dt)\}^+\text{-Ph-}\{NDI^-\}]^*$, persists on a time-scale longer than the time-scale of the TRIR and ultrafast TA experiments, both of which are limited to about 2 ns, nanosecond TA spectroscopy was performed using 30-ps Nd:YAG laser and diode registration, for a solution of **2** (ca. 1 mM) in CH_2Cl_2 at room temperature (r.t.). This experiment yielded a value for the lifetime of the charge-separated state of 15 (±3) ns, together with a minor (<10%) component which did not decay on the time scale of the experiment.

DISCUSSION

Figure 12 summarizes the photophysical events observed following the excitation of a solution of **2** (ca. 1 mM) in CH_2Cl_2 by a 400 or a 383 nm ~120 fs laser pulse. This diagram includes the formation and recombination of the charge-separated state $[Cp_2\{Mo(dt)^+\}\text{-Ph-}\{NDI\}^-]$ the energy of which, as estimated from the difference between the potentials of first oxidation (−0.31 V) and the first reduction (−0.97 V) processes of **2** in DMF (Table 1), is 0.66 eV. Given the anticipated solvatochromism of the charge-separated state, this value may be somewhat higher in CH_2Cl_2 than in DMF.

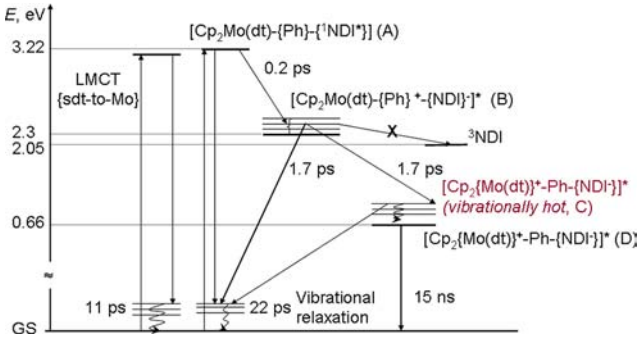

Figure 12. Summary of photophysical processes of a solution of **2** (ca. 1 mM) in CH_2Cl_2 following 400 or 383 nm, ~120 fs excitation. Where both TRIR and TA were used to monitor a particular process, the lifetime stated is an average from the values obtained. This diagram was constructed using the following energies: ^{1}NDI* 3.22 eV; ^{3}NDI 2.05 eV (which were averaged from the sources[77−80]), and Ph→NDI ^{1}CT 2.3 eV estimated as the mean value between the energy of the charge-transfer emission band in the room temperature fluorescence spectrum of *N*-isooctyl-*N*′-Ph-NDI[74] and the combination of redox potentials (see text for details). A, B, C, and D correspond to the sequence of the states described in Figure 10a.

Excitation of **2** by 400 or 383 nm light leads to the population of an NDI excited state and the metalladithiolene-based excited states derived from the ene-1,2-dithiolate→Mo and sulfur→Mo LMCT transitions. Our studies indicate that the LMCT excited states decay to the ground state without engaging in any charge transfer processes. However, the population of an NDI excited state leads to a spectrum which strongly resembles that of asymmetric *N*-isooctyl-*N*′-Ph-NDI[74a] and is attributed to ^{1}NDI*. Our studies indicate that the initial ^{1}NDI* state undergoes an ultrafast Ph→NDI electron transfer to form the local charge-transfer excited state $[Cp_2Mo(dt)\text{-}\{Ph\}^+\text{-}\{NDI\}^-]$. The TA spectrum of this second excited state (green spectrum in Figure 10) closely resembles that observed for *N*-isooctyl-*N*′-Ph-NDI which was assigned to a charge-transfer from Ph to NDI excited state, $[N\text{-isooctyl-}N'\text{-}\{Ph\}^+\text{-}\{NDI\}^-]$.[74a] Given the highly energetic initial ^{1}NDI* state (3.22 eV) the formation of $[Cp_2Mo(dt)\text{-}\{Ph\}^+\text{-}\{NDI\}^-]$ state in **2** should be thermodynamically allowed. The energy of $[Cp_2Mo(dt)\text{-}\{Ph\}^+\text{-}\{NDI\}^-]$ state can be estimated in two ways. The lower limit is given by the maximum of the emission band attributed to the charge transfer emission of $[N\text{-isooctyl-}N'\text{-}\{Ph\}^+\text{-}\{NDI\}^-]$[74a] (ca. 2.2 eV). On the other hand, the difference between the first oxidation potential of *p*-xylene (2.01 V vs SCE, i.e., about 1.5 V vs Fc^+/Fc)[91] and the first reduction potential of **2** (−0.97 V vs Fc^+/Fc) yields the upper limit of 2.47 eV for the energy of the $[Cp_2Mo(dt)\text{-}\{Ph\}^+\text{-}\{NDI\}^-]$ state. The average value of 2.3 eV has been used for

Figure 12. While a large range of phenyl-bridged molecular systems designed for photoinduced electron transfer has been reported,[74b−f] where phenyl units act solely as a mediator in the superexchange mechanism rather than being directly involved in the process of charge-separation (perhaps partly because the energy of the initially populated excited states in such systems may not be sufficient to oxidize the phenyl unit), we note that the rate of charge transfer across the phenyl group in such systems is comparatively slow, no faster than 1−2 ps, and most commonly, about tens of ps. However, in **2**, we observe a formation of the features characteristic of the NDI-anion within 0.2 ps (green spectrum in Figure 10a), and consider this difference in the rates as an additional proof that in **2**, the first ultrafast step of charge separation involves oxidation of the phenyl unit. While the direct spectroscopic features of a Ph-cation cannot be detected in our experiments, it is not illogical to assume that, given it is thermodynamically possible, the Ph-group is being oxidized by ^{1}NDI* as a first step of charge separation. Ganesan et al. postulated the formation of such a charge-transfer excited state.[74a]

The charge transfer Ph→NDI to form $[Cp_2Mo(dt)\text{-}\{Ph\}^+\text{-}\{NDI\}^-]$ represents the first step in a cascade electron transfer process. As indicated by the results of both TRIR and TA spectroscopic investigations (vide ultra), this state has a lifetime of about 1.7 ps (an average of the respective values of 1.88 and 1.47 ps). The $[Cp_2Mo(dt)\text{-}\{Ph\}^+\text{-}\{NDI\}^-]$ has two major decay routes: a production of a vibrationally hot ground state, or further electron transfer involving oxidation of the ene-1,2-dithiolate moiety and reduction of the Ph$^+$ moiety to form the $[Cp_2\{Mo(dt)\}^+\text{-Ph-}\{NDI\}^-]$ charge-separated state. This process of charge separation is accompanied by a loss of about 1.6 eV in energy, as estimated from the difference in the corresponding redox potentials.

The 22−24 ps process is observed in both the TRIR and the TA data. In the TRIR, it is attributed to a decay of vibrationally hot NDI-based states, both in the ground state and in the charge-separated state involving NDI$^-$ anion. In the TA spectra, the 24 ps component corresponds to the final transformation from the third excited state (Figure 10a, state C, vibrationally hot $[Cp_2\{Mo(dt)\}^+\text{-Ph-}\{NDI\}^-]$) to the final excited state (D) which persists into the nanosecond domain. The spectra of C and D are similar and only differ in their intensities; about 50% of the NDI$^-$ anion absorbance in C is present in D. One possibility is that once the $[(Cp)_2\{Mo(dt)\}^+\text{-Ph-}\{NDI\}^-]$ charge-separated state is formed vibrationally hot within the 1.7 ps formation time, then a decay into the ground state is possible from this hot state, with the rate of 22 ps being concomitant with the vibrational cooling process. However, once vibrationally relaxed, decay to the ground state is not possible (perhaps because of an activation barrier) and hence the amount of the $[(Cp)_2\{Mo(dt)\}^+\text{-Ph-}\{NDI\}^-]$ charge separated state remaining persists on the nanosecond time-scale. Given the relative intensities of the excited states (Figure 10), this final channel of repopulating hot ground state from the hot charge separated state would amount for <10% of the hot NDI and, as it occurs with the same rate as vibrational cooling, this would not be detected as a separate process in the TRIR experiments.

The final $[Cp_2Mo(dt)\text{-}\{Ph\}^+\text{-}\{NDI\}^-]$ charge separated state of **2** has a lifetime of 15 ns.

CONCLUSIONS

We have accomplished the synthesis, characterization, and investigations—including a detailed photophysical study—of the first example of a charge-separated dyad which involves a molybdenum ene-1,2-dithiolate complex. A new pro-ligand, containing a protected ene-1,2-dithiolate bound through a phenyl linkage to an electron acceptor, naphthalenetetracarboxylicdiimide (NDI) group, has been synthesized. Deprotection of this pro-ligand by base hydrolysis, followed by reaction with $[Cp_2MoCl_2]$, produced the new Donor−Acceptor dyad $[Cp_2Mo(SC(H)C(C_6H_4\text{−NDI})S)]$ (**2**). Electrochemical investigations showed that **2** can be reversibly oxidized to $[\mathbf{2}]^+$ and reduced to $[\mathbf{2}]^-$, $[\mathbf{2}]^{2-}$, and $[\mathbf{2}]^{3-}$. These studies, augmented by UV/vis, EPR, and IR spectroscopic investigations of these species, showed that the HOMO of **2** is ene-1,2-dithiolate based and the LUMO is NDI-based, conclusions that are supported by DFT calculations for the electronic ground state of **2**. The spectroscopic and electrochemical data suggest that, in the electronic ground state of **2**, $\{Cp_2Mo(dithiolene)\}$ and $\{NDI\}$ act as two essentially independent functionalities, in agreement with the results of the DFT calculations.

The dynamics of the excited states of **2** in CH_2Cl_2 solution were investigated by time-resolved IR spectroscopy following irradiation by a 400 nm ∼120 fs laser pulse. These investigations were complemented by an ultrafast TA spectroscopic study of **2** in CH_2Cl_2 solution following irradiation by a 383 nm ∼120 fs laser pulse. These studies showed that irradiation of **2** at both 400 and 383 nm leads to the formation of the $[(Cp)_2\{Mo(dt)\}^+\text{-Ph-}\{NDI\}^-]$ charge-separated state as a result of a cascade electron transfer initiated by the formation of an ^{1}NDI* excited state. ^{1}NDI* rapidly (ca. 0.2 ps) forms the charge transfer state $[Cp_2Mo(dt)\text{-}\{Ph\}^+\text{-}\{NDI\}^-]$ which has a lifetime of about 1.7 ps and decays to produce the ground state and the $[(Cp)_2\{Mo(dt)\}^{+\cdot}\text{-Ph-}\{NDI\}^-]$ charge-separated state; the latter has an appreciable lifetime, about 15 ns in CH_2Cl_2 at room temperature.

We hope that the generation of the $[(Cp)_2\{Mo(dt)\}^+\text{-Ph-}\{NDI\}^-]$ charge-separated state in this metalla-ene-1,2-dithiolate-spacer-imide D−A dyad encourages further such studies, not least because of the considerable range and diversity of metal-ene-1,2-dithiolate complexes that are available.[18] Further potential developments of this chemistry could include tuning the rates of charge separation and charge recombination by varying the electron donating properties of the donor, the electron withdrawing properties of the acceptor or the nature of the spacer group. Given the successes accomplished with other charge-transfer dyads and triads, including Pt(II)-dithiolene complexes,[11,25] we are optimistic that new molybdenum-based compounds will be produced possessing such properties; some of these may be suitable for strategically valuable applications, for example, the generation of electrical energy from sunlight or photocatalysis for the production of hydrogen from water.

EXPERIMENTAL SECTION

^{1}H NMR spectra were recorded using either a Bruker DPX300 spectrometer or a Jeol 270 spectrometer. Mass spectrometric data were recorded on a Bruker MicroTOF (ESI) or a Micromass 70E (EI) instrument. EPR spectra were recorded on a Bruker EMX spectrometer fitted with a frequency counter and spectral simulations were accomplished using WINEPR SimFonia v1.25 software, Bruker Analytische Messtechnik GmbH. The concentration of the samples for EPR studies obtained by bulk electrolysis was about 1 mM. Standard

IR spectra were recorded on a Nicolet Avatar 360 FT-IR spectrometer. Elemental analyses were conducted by the University of Nottingham, School of Chemistry, Microanalytical Service, and by the Elemental Analysis Service at London Metropolitan University.

Cyclic voltammetric and coulometric studies were carried out using an Autolab PGSTAT20 potentiostat. The cyclic voltammetry was carried out under an atmosphere of argon using a three-electrode arrangement in a single compartment cell, a glassy carbon working electrode, a Pt wire secondary electrode, and a saturated calomel reference electrode, chemically isolated from the test solution via a bridge tube containing electrolyte solution and fitted with a porous vycor frit. The solutions were 10^{-3} M in the test compound unless stated otherwise; $[^{n}Bu_4N][BF_4]$ (0.2 M) was used as the supporting electrolyte. The redox potentials are quoted versus the ferrocenium-ferrocene (Fc^{+}/Fc) couple.

Coulometric studies, at a controlled potential, were carried out using a two-compartment cell. The Pt/Rh gauze basket working electrode was separated from the wound Pt/Rh gauze secondary electrode by a glass frit. A saturated calomel reference electrode was bridged to the test solution through a vycor frit orientated at the center of the working electrode. The working electrode compartment was fitted with a magnetic stirrer bar, and the test solution was stirred rapidly during electrolysis. The UV/vis spectroelectrochemical experiments were carried out on about 0.5 mM solutions in an optically transparent electrochemical (OTE) cell (modified quartz cuvette, with 0.5 mm optical path length).[81] The cell comprised a three-electrode configuration, consisting of a Pt/Rh gauze working electrode, a Pt wire secondary electrode (in a fritted PTFE sleeve), and a saturated calomel electrode, chemically isolated from the test solution via a bridge tube containing electrolyte solution and terminated in a porous frit. The potential at the working electrode was controlled by a Sycopel Scientific Ltd. DD10 M potentiostat. The (spectro)electrochemical UV/vis data were recorded on a Perkin-Elmer Lambda 16 spectrophotometer. The cavity was purged with dinitrogen, and temperature control at the sample was achieved by flowing cooled dinitrogen across the surface of the cell.

Picosecond TA experiments were performed at the B. I. Stepanov Institute of Physics, Minsk, on a pump−probe spectrometer based on a homemade original fs Ti:Sapph pulsed oscillator and regenerative amplifier system operated at a 10 Hz repetition rate.[82] The Ti:Sapph master oscillator was synchronously pumped with doubled output of a homemade mode-locked picosecond pulsed Nd:YAG laser. The regenerative amplifier was pumped with a ns Q-switched Nd:YAG laser LS-2134 (LOTIS TII). The pulse width and energy of the Ti:Sapph system after the amplifier were about 150 fs and 0.5 mJ, respectively, tunable over the spectral range 760−820 nm. The fundamental output of the Ti:Sapph system (766 nm output wavelength was set for the present study) was split into two beams with an intensity ratio of 1:4. The more intense beam was passed through a controlled delay line and after frequency doubling (to provide 383 nm radiation) was utilized for sample pumping. The energy of 383 nm pump pulses was about 40 μJ and was focused to a 500 × 500 μm spot on the sample. The second beam of the fundamental frequency was used for generation of a femtosecond supercontinuum (by focusing into a 1 cm path length cell containing water) which served as the probe radiation. The continuum probe light was split with a beam splitter into two pulses (reference and signal), identical in intensity, and the signal was focused on the sample by mirror optics. The spectra of both pulses were recorded for each laser flash by a polychromator equipped with CCD camera and transferred to the computer. The time resolution of the setup is limited by the pump and probe pulse duration and estimated as about 0.2 ps. A solution of **2** in CH_2Cl_2 was flowed through a 5-mm quartz cell during the course of the experiment.

Picosecond TRIR studies were performed in the Ultrafast Spectroscopy Laboratory, Rutherford Appleton Laboratory, STFC, UK, ULTRA[83] facility, a cluster of sensitive ultrafast IR and Raman spectrometers. The IR spectrometer comprised two synchronized 10 kHz, 8 W, 40 fs and 2 ps titanium sapphire oscillator/regenerative amplifiers (Thales) which pump a range of optical parametric amplifiers (TOPAS). A portion of the 40 fs Ti:S beam was used to generate tunable mid-IR probe light with around 400 cm^{-1} bandwidth. The 400 nm pump beam was generated from the second harmonic of the 40 fs laser. The probe and pump beam diameters in the sample were about 70 and 120 μm, respectively, and the pump energy at the sample was 1 to 1.5 μJ. In this case changes in IR absorption spectra were recorded by three HgCdTe linear-IR array detectors on a shot-by-shot basis. All experiments were carried out in Harrick cells with 2 mm thick CaF_2 windows with 500 to 950 μm sample path length and a typical optical density of 0.5 to 1 at 400 nm. All samples were mounted on a 2D-raster stage and solutions were flowed through the cell to ensure photostability.

Nanosecond TA studies were performed using a home-built setup in Sheffield. The third harmonic (355 nm) of a picosecond Nd:YAG laser (PY61−10, Continuum) was used as the excitation source, with the excitation pulse energy at the sample attenuated to 1 mJ to avoid nonlinear sample response. The changes in absorbance of the photoexcited sample were probed by a pulsed Xe arc lamp (Applied Photophysics, 150 W). A Si PIN photodiode detector (DET10A/M, Thorlabs) coupled to a digital oscilloscope (Tektronix TDS 3032B) was used to monitor the changes in the probe light intensity. The spectral selectivity of the detection system was achieved using narrow band-pass filters (CVI Technical Optics or Thorlabs, spectral bandwidth 10−12 nm). The home-built delay-generator/trigger-suppressor electronic unit was used to synchronize the slow pulse rate of the Xe lamp (0.3 Hz) with the repetition rate of the picosecond laser (10 Hz). For fine adjustment of the timing of the Xe lamp pulses, a digital delay generator was employed (Princeton Applied Research, Model 4144). An electro-mechanical beam shutter (SH05, Thorlabs) was placed in the excitation beam to avoid unnecessary sample irradiation by unused excitation pulses. Each of the measurements was performed in a quartz cells with 1 mm path length. The overall time resolution of the detection system is estimated as about 1.8 ns fwhm.

Analysis of time-resolved data to obtain decay lifetimes was performed using Igor Pro software (WaveMetrics, Inc.). The decay kinetics were fitted to the sum of exponentials (with an addition of a long-lived component if required) using a least-squares algorithm built into Igor Pro. In the case of picosecond TA data, a deconvolution of the instrumental response (approximated as a Gaussian profile of several hundred fs fwhm) from the experimental decay kinetics was applied. The determination of actual zero time delay for each spectral position was incorporated in the data analysis algorithm, which automatically provided chirp correction. For picosecond TA and TRIR data, global fitting (the option available in Igor Pro) was applied to analyze simultaneously the decay kinetics obtained for a number of spectral points. This approach considerably increased reliability of the lifetimes obtained, and also provided the individual spectra of intermediate species associated with each decay time in case of TA data. To perform the global fitting for picosecond TA data, the number of decay traces was obtained across the available spectral range by integrating 10 nm wide spectra slices. TRIR data were considered per pixel (without averaging), and the pixels comprising the main bands were used in the Igor Pro global fit. Spectral shifts were taken into account as additional kinetic components in the fit. In addition, separate kinetic traces were fitted individually (Origin 8.5), to check the consistency of the fit.

Restricted DFT calculations were performed using the Amsterdam Density Functional (ADF) suite version 2010.01.[84,85] The DFT calculations employed a Slater-type orbital (STO) all-electron triple-ζ-plus one polarization function basis set from the ZORA/TZP database of the ADF suite for all atoms. The scalar relativistic (SR) approach was used within the ZORA Hamiltonian for the inclusion of relativistic effects and the local density approximation (LDA) with the correlation potential due to Vosko et al.[86] was used in the gas phase geometry optimizations of the model of **2**. Gradient corrections were performed using the functionals of Becke[87] and Perdew (BP).[88] Coordinates for the model of **2** were derived from gas phase geometry optimizations of models of $[Cp_2Mo(dt\text{-}Ph)]$ that we have reported previously.[43] The gas phase geometry optimization employed a truncated model of **2** in which the 2-(ethyl)-hexyl group pendant to the NDI unit was replaced

with a methyl group. The coordinate frame employed in the calculations is shown in Figure 6, and the geometry optimized coordinates for the model of **2** are given in the Supporting Information (Supporting Information, Table SI3). The *z*-axis bisects the S-M-S angle, and the *x*-axis lies in the MoS_2 plane. Pictorial representations of the MOs were generated using MOLEKEL,[89] and the spectrum was calculated using SWIZARD.[90]

Synthesis of 1-(Phenyl-4-*N*-(2-ethylhexyl)-naphthalene-diimide) Ethanone. *N*-(2-ethylhexyl)-1,4,5,8-naphthalene tetracarboxylic monoanhydride[65] (4.27 g, 11.3 mmol) and 4-aminoacetophenone (1.68 g, 12.4 mmol) were heated at reflux under argon in dry DMF (20 cm^3) for 24 h. The solution was cooled to room temperature and the product precipitated with the addition of diethylether (20 cm^3). The precipitate was collected by filtration and dried under a reduced pressure to produce a pale cream solid (2.43 g, 43%). Analysis calculated for $C_{30}H_{28}N_2O_5$: Expected (Found): C 72.56 (72.49), H 5.68 (5.57), N 5.64 (5.69). ^{1}H NMR (270 MHz, $CDCl_3$): δ_H 8.77 (s, 4H, H^{naph}), 8.15 (d, 2H, H^{Ph}, $^3J_{H,H}$ = 8.6 Hz), 7.44 (d, 2H, H^{Ph}, $^3J_{H,H}$ = 8.6 Hz), 4.13 (m, 2H, NCH_2,), 2.86 (s, 3H, $C(O)CH_3$), 1.96 (m, 1H, $C(H)(CH_2CH_3)((CH_2)_3CH_3)$), 1.50−1.20 (m, 8H, $C(H)(CH_2CH_3)((CH_2)_3CH_3)$), 1.00−0.80 (m, 6H, $C(H)(CH_2CH_3)((CH_2)_3CH_3)$). Mass Spectrometry ($EI^+$): m/z $[C_{30}H_{28}N_2O_5]^+$ 496.2001

Synthesis of 2-Bromo-1-(phenyl-4-*N*-(2-ethylhexyl)-naphthalene-diimide) Ethanone. 1-(Phenyl-4-*N*-(2-ethylhexyl)-naphthalene-diimide)ethanone (2.00 g, 4.0 mmol) and bromine (0.64 g, 4.0 mmol) were stirred together for 3 h at 60 °C in acetic acid (150 cm^3). After this time further bromine (0.64 g, 4.0 mmol) was added, and the mixture stirred for 3 h at 60 °C. The mixture was cooled to room temperature, and the precipitate that formed was collected by filtration. Deionized water (100 cm^3) was added to the filtrate causing further precipitation, and the solid was collected by filtration. The product was separated by column chromatography using a mixture of solvents as an eluant (95 cm^3 CH_2Cl_2, 5 cm^3 ethyl acetate, 20 drops of methanol) over a silca gel support (Kieselgel 60, 220−240 mesh) leaving a pale cream solid (0.50 g, 21%). Analysis calculated for $C_{30}H_{27}BrN_2O_5$: Expected (Found): C 62.62 (62.54), H 4.73 (4.72), N 4.87 (4.85). ^{1}H NMR (300 MHz, $CDCl_3$): δ_H 8.82 (s, 4H, H^{naph}), 8.21 (d, 2H, H^{Ph}, $^3J_{H,H}$ = 6.6 Hz), 7.50 (d, 2H, H^{Ph}, $^3J_{H,H}$ = 6.6 Hz), 4.51 (s, 2H, CH_2Br), 4.18 (m, 2H, NCH_2,), 1.98 (m, 1H, $C(H)(CH_2CH_3)((CH_2)_3CH_3)$), 1.50−1.25 (m, 8H, $C(H)(CH_2CH_3)((CH_2)_3CH_3)$), 1.05−0.85 (m, 6H, $C(H)(CH_2CH_3)((CH_2)_3CH_3)$). Mass Spectrometry ($EI^+$): m/z $[C_{30}H_{27}BrN_2O_5]^+$ 574.1130

Synthesis of *S*-2-(4-Phenyl-*N*-(2-ethylhexyl)-naphthalene-diimide)-2-oxoethyl *O*-isopropylcarbondithioate. 2-Bromo-1-(phenyl-4-*N*-(2-ethylhexyl)-naphthalene-diimide)ethanone (0.98 g, 1.7 mmol) and potassium *O*-isopropylxanthate (0.36 g, 2.1 mmol) were stirred together in CH_2Cl_2 (50 cm^3) for 3 h. Deionized water (50 cm^3) was added to quench the reaction and the CH_2Cl_2 phase separated. The aqueous phase was washed with CH_2Cl_2 (3 × 15 cm^3); the CH_2Cl_2 extracts were combined, dried over anhydrous $MgSO_4$; the mixture was filtered, and the solvent evaporated from the filtrate under a reduced pressure to produce a yellow solid (1.05 g, 98%). Analysis calculated for $C_{34}H_{34}N_2O_6S_2$; Expected (Found): C 64.74 (64.67), H 5.43 (5.38), N 4.44 (4.35). ^{1}H NMR (270 MHz, $CDCl_3$): δ_H 8.83 (s, 4H, H^{naph}), 8.25 (d, 2H, H^{Ph}, $^3J_{H,H}$ = 6.5 Hz), 7.51 (d, 2H, H^{Ph}, $^3J_{H,H}$ = 6.5 Hz), 5.73 (sept, 1H, $C(H)(CH_3)_2$, $^3J_{H,H}$ = 6.2 Hz), 4.70 (s, 2H, $C(O)CH_2S$), 4.16 (m, 2H, NCH_2), 1.95 (m, 1H, $C(H)(CH_2CH_3)((CH_2)_3CH_3)$), 1.50−1.25 (m, 14H, $C(H)(CH_3)_2$ + $C(H)(CH_2CH_3)((CH_2)_3CH_3)$), 1.05−0.85 (m, 6H, $C(H)(CH_2CH_3)((CH_2)_3CH_3)$). Mass Spectrometry ($ESI^+$): m/z $[C_{34}H_{34}N_2O_6S_2]$ + (Na^+ 653.1756), (H^+ 631.1938).

Synthesis of 4-(4-Phenyl-*N*-(2-ethylhexyl)-naphthalene-diimide)-1,3-dithiol-2-one (1). *S*-2-(4-phenyl-*N*-(2-ethylhexyl)-naphthalene-diimide)-2-oxoethyl *O*-isopropylcarbondithioate (1.00 g, 1.6 mmol) was dissolved in H_2SO_4 (10 cm^3, 98%). After 5 min, ice was added until no further heat was generated; then the mixture was diluted with deionized water to about 250 cm^3 and neutralized with $NaHCO_3$. CH_2Cl_2 (100 cm^3) was added and the CH_2Cl_2 phase separated. The aqueous phase was washed with CH_2Cl_2 (3 × 50 cm^3). The CH_2Cl_2 extracts were combined, dried over anhydrous $MgSO_4$; the mixture was filtered and the solvent evaporated from the filtrate under a reduced pressure to produce a sparingly soluble red solid (0.86 g, 95%). Analysis calculated for $C_{31}H_{26}N_2O_5S_2$: Expected (Found): C 65.24 (65.31), H 4.59 (4.64), N 4.91 (4.87). ^{1}H NMR (270 MHz, $CDCl_3$): δ_H 8.84 (s, 4H, H^{naph}), 7.65 (d, 2H, H^{Ph}, $^3J_{H,H}$ = 8.4 Hz), 7.41 (d, 2H, H^{Ph}, $^3J_{H,H}$ = 8.4 Hz), 6.96 (s, 1H, H^{dithio}), 4.17 (m, 2H, NCH_2,), 1.95 (m, 1H, $C(H)(CH_2CH_3)((CH_2)_3CH_3)$), 1.50−1.20 (m, 8H, $C(H)(CH_2CH_3)((CH_2)_3CH_3)$), 1.00−0.80 (m, 6H, $C(H)(CH_2CH_3)((CH_2)_3CH_3)$). Mass Spectrometry ($EI^+$): m/z $[C_{31}H_{26}N_2O_5S_2]^+$ 570.1265

Synthesis of [Cp_2Mo(dt-Ph-NDI)] (2). 4-(4-Phenyl-*N*-(2-ethylhexyl)-naphthalene diimide)-1,3-dithiol-2-one (100 mg, 0.18 mmol) was dissolved in H_2SO_4 (2 cm^3, 98%), the solution was diluted with deionized water (25 cm^3), and the compound extracted into CH_2Cl_2 (25 cm^3). Anhydrous methanol (10 cm^3) and cesium hydroxide (38 mg, 0.35 mmol) were added and the mixture stirred under argon for 30 min. Bis(cyclopentadienyl)molybdenum dichloride (57 mg, 0.19 mmol) was added and the solution stirred overnight; the solvent was removed under a reduced pressure producing a dark brown solid. The pure product was separated by column chromatography using 90% CH_2Cl_2 and 10% ethyl acetate as the eluant over silica gel (Kieselgel 60, 220−240 mesh) to produce a brown solid (27 mg, 18%). Elemental Analysis for $C_{40}H_{36}MoN_2O_4S_2$; Expected (Found): C 62.49 (62.42), H 4.72 (4.68), N 3.64 (3.59). ^{1}H NMR (270 MHz, $CDCl_3$): δ_H 8.80 (s, 4H, H^{naph}), 7.87 (d, 2H, H^{Ph}, $^3J_{H-H}$ 8.1 Hz), 7.18 (d, 2H, H^{Ph}, $^3J_{H-H}$ 8.1 Hz), 6.93 (s, br, 1H, H^{dithio}), 5.32 (s, 10H, Cp), 4.18 (m, 2H, NCH_2,), 2.02 (m, 1H, $C(H)(CH_2CH_3)((CH_2)_3CH_3)$), 1.50−1.20 (m, 8H, $C(H)(CH_2CH_3)((CH_2)_3CH_3)$), 1.00−0.80 (m, 6H, $C(H)(CH_2CH_3)((CH_2)_3CH_3)$). Mass Spectrometry (ESI): m/z $[C_{40}H_{36}MoN_2O_4S_2]$ 770.1172.

■ ASSOCIATED CONTENT

Ⓢ Supporting Information

Further details are given in Figures SI1−SI6 and Tables SI1−SI3. This material is available free of charge via the Internet at http://pubs.acs.org.

■ AUTHOR INFORMATION

Corresponding Author

*E-mail: Dave.Garner@Nottingham.ac.uk (C.D.G.); E.S.Davies@nottingham.ac.uk (E.S.D.); Julia.Weinstein@Sheffield.ac.uk (J.A.W.).

Notes

The authors declare no competing financial interest.

■ ACKNOWLEDGMENTS

We thank the Engineering and Physical Sciences Research Council, U.K., the Royal Society, U.K., and BRFFR, Belarus (F11_IC-030), for funding and the Rutherford Appleton Laboratory, Science and Technology Funding Council, U.K. for TRIR beam time. We thank the Universities of Nottingham and Sheffield for their support.

■ REFERENCES

(1) Vlček, A. *Coord. Chem. Rev.* **2000**, *200*, 933−977.
(2) Falkenström, M.; Johansson, O.; Hammarström, L. *Inorg. Chim. Acta* **2007**, *360*, 741−750.
(3) Balzani, V.; Venturi, M.; Credi, A. *Molecular Devices and Machines*, 2nd ed.; Wiley-VCH: Weinheim, Germany, 2008; p 546.
(4) Eisenberg, R. *Science* **2009**, *324*, 44−45.
(5) Alstrum-Acevedo, J. H.; Brennaman, M. K.; Meyer, T. J. *Inorg. Chem.* **2005**, *44*, 6802−6827.
(6) Solar energy forum articles, *Inorg. Chem.*, **2005**, *44*, 6799−7260.
(7) Lei, P.; Hedlund, M.; Lomoth, R.; Rensmo, H.; Johansson, O.; Hammarström, L. *J. Am. Chem. Soc.* **2008**, *130*, 26−27.

(8) Ozawa, H.; Sakai, K. *Chem. Commun.* **2011**, *47*, 2227−2242. Ozawa, H.; Haga, M. A.; Sakai, K. *J. Am. Chem. Soc.* **2006**, *128*, 4926−4927. Sakai, K.; Ozawa, H. *Coord. Chem. Rev.* **2007**, *251*, 2753−2766.
(9) Geary, E. A. M.; Yellowlees, L. J.; Jack, L. A.; Oswald, I. D. H.; Parsons, S.; Hirata, N.; Durrant, J. R.; Robertson, N. *Inorg. Chem.* **2005**, *44*, 242−250.
(10) Du, P.; Schneider, J.; Li, F.; Zhao, W.; Patel, U.; Castellano, F. N.; Eisenberg, R. *J. Am. Chem. Soc.* **2008**, *130*, 5056−5058. Chakraborty, S.; Wadas, T. J.; Hester, H.; Flaschenreim, C.; Schmehl, R.; Eisenberg, R. *Inorg. Chem.* **2005**, *44*, 6284−6293. Schneider, J.; Du, P.; Wang, X.; Brennessel, W. W.; Eisenberg, R. *Inorg. Chem.* **2009**, *48*, 1498−1506. Du, P.; Schneider, J.; Jarosz, P.; Zhang, J.; Brennessel, W. W.; Eisenberg, R. *J. Phys. Chem. B* **2007**, *111*, 6887−6894.
(11) Lazarides, T.; McCormick, T. M.; Wilson, K. C.; Lee, S.; McCamant, D. W.; Eisenberg, R. *J. Am. Chem. Soc.* **2011**, *133*, 350−364.
(12) Kwok, E. C. -H.; Chan, M.-Y.; Wong, K. M. -C.; Lam, W. H.; Yam, V. W. -W. *Chem.—Eur. J.* **2010**, *16*, 12244−12254.
(13) Weinstein, J. A.; Zheligovskaya, N. N.; Mel'nikov, M. Y.; Hartl, F. *J. Chem. Soc., Dalton Trans.* **1998**, 2459−2466. Weinstein, J. A.; Zheligovskaya, N. N.; Lileev, I. V.; Galin, A. M.; Mel'nikov, M. Y. *Russ. J. Inorg. Chem. (Transl. of Zh. Neorg. Khim.)* **1998**, *43*, 1361−1367. Weinstein, J. A.; Tierney, M. T.; Davies, E. S.; Base, K.; Robeiro, A. A.; Grinstaff, M. W. *Inorg. Chem.* **2006**, *45*, 4544−4555.
(14) Wang, X.; Goeb, S.; Ji, Z.; Pogulaichenko, N. A.; Castellano, F. N. *Inorg. Chem.* **2011**, *50*, 705−707.
(15) Muro, M. L.; Rachford, A. A.; Wang, X.; Castellano, F. N. *Top. Organomet. Chem.* **2010**, *29*, 159−191.
(16) Archer, S.; Weinstein, J. A. *Coord. Chem. Rev.* **2012**, *256*, 2530−2561.
(17) McCleverty, J. A. *Prog. Inorg. Chem.* **1968**, *10*, 49−221.
(18) *Dithiolene Chemistry: Synthesis, Properties and Applications*; Stiefel, E. I., Ed.; Wiley: Hoboken, NJ, 2004.
(19) Fourmigué, M. *Acc. Chem. Res.* **2004**, *37*, 179−186.
(20) Sproules, S.; Weyhermüller, T.; DeBeer, S.; Wieghardt, K. *Inorg. Chem.* **2010**, *49*, 5241−5261.
(21) Garreau-de Bonneval, B.; Moineau-Chane Ching, K. I.; Alary, F.; Bui, T.-T.; Valade, L. *Coord. Chem. Rev.* **2010**, *254*, 1457−1467.
(22) Kusamoto, T.; Kume, S.; Nishihara, H. *J. Am. Chem. Soc.* **2008**, *130*, 13844−13845.
(23) McCall, K. L.; Morandeira, A.; Durrant, J.; Yellowlees, L. J.; Robertson, N. *Dalton Trans.* **2010**, *39*, 4138−4145.
(24) Ishikawa, T.; Fukazawa, N.; Matsubara, Y.; Nakajima, R.; Onda, K.; Okimoto, Y.; Koshihara, S.; Lorenc, M.; Collet, E.; Tamura, M.; Kato, R. *Phys. Rev. B* **2009**, *80*, 115108.
(25) Zuleta, J. A.; Bevilacqua, J. M.; Rehm, J. M.; Eisenberg, R. *Inorg. Chem.* **1992**, *31*, 1332−1337.
(26) Tamura, M.; Takenaka, K.; Takagi, H.; Sugai, S.; Tajima, A.; Kato, R. *Chem. Phys. Lett.* **2005**, *411*, 133−137.
(27) Canevet, D.; Sallé, M.; Zhang, G.; Zhang, D.; Zhu, D. *Chem. Commun.* **2009**, 2245−2269.
(28) Kreher, D.; Hudhomme, P.; Gorgues, A.; Luo, H.; Araki, Y.; Ito, O. *Phys. Chem. Chem. Phys.* **2003**, *5*, 4583−4592.
(29) Martín, N.; Sánchez, L.; Herranz, M. A.; Guldi, D. M. *J. Phys. Chem. A* **2000**, *104*, 4648−4657.
(30) Allard, E.; Cousseau, J.; Ordúna, J.; Garín, J.; Luo, H.; Araki, Y.; Ito, O. *Phys. Chem. Chem. Phys.* **2002**, *4*, 5944−5951.
(31) Kodis, G.; Liddell, P. A.; de la Garza, L.; Moore, A. L.; Moore, T. A.; Gust, D. *J. Mater. Chem.* **2002**, *12*, 2100−2108.
(32) Nielsen, K. A.; Levillain, E.; Lynch, V. M.; Sessler, J. L.; Jeppesen, J. O. *Chem.—Eur. J.* **2009**, *15*, 506−516.
(33) Becher, J.; Brimert, T.; Jeppesen, J. O.; Pedersen, J. Z.; Zubarev, R.; Bjørnholm, T.; Reitzel, N.; Jensen, T. R.; Kjaer, K.; Levillain, E. *Angew. Chem., Int. Ed.* **2001**, *40*, 2497−2500.
(34) El-Kouly, M. E.; Jaggi, M.; Schmid, B.; Blum, C.; Liu, S.-X.; Decurtins, S.; Ohkubo, K.; Fukuzumi, S. *J. Phys. Chem C* **2011**, *115*, 8325−8334.
(35) Matsuo, Y.; Maruyama, M.; Gayathri, S. S.; Uchida, T.; Guldi, D. M.; Kishida, H.; Nakamura, A.; Nakamura, E. *J. Am. Chem. Soc.* **2009**, *131*, 12643−12649.
(36) Grätzel, M. *Inorg. Chem.* **2005**, *44*, 6841−6851.
(37) Wright, R. J.; Lim, C.; Tilley, T. D. *Chem.—Eur. J.* **2009**, *15*, 8518−8525.
(38) Samuel, A. P. S.; Co, D. T.; Stern, C. L.; Wasielewski, M. R. *J. Am. Chem. Soc.* **2010**, *132*, 8813−8815.
(39) Fourmigué, M.; Domercq, B.; Jourdain, I. V.; Molinié, P.; Guyon, F.; Amaudrut, J. *Chem.—Eur. J.* **1998**, *4*, 1714−1723.
(40) Clérac, R.; Fourmigué, M.; Coulon, C. *J. Solid State Chem.* **2001**, *159*, 413−419.
(41) Domercq, B.; Coulon, C.; Fourmigué, M. *Inorg. Chem.* **2001**, *40*, 371−378.
(42) Hsu, J. K.; Bonangelino, C. J.; Kaiwar, S. P.; Boggs, C. M.; Fettinger, J. C.; Pilato, R. S. *Inorg. Chem.* **1996**, *35*, 4743−4751.
(43) Whalley, A. L.; Blake, A. J.; Collison, D.; Davies, E. S.; Disley, H. J.; Helliwell, M.; Mabbs, F. E.; McMaster, J.; Wilson, C.; Garner, C. D. *Dalton Trans.* **2011**, *40*, 10457−10472.
(44) Fourmigué, M.; Lenoir, C.; Coulon, C.; Guyon, F.; Amaudrut, J. *Inorg. Chem.* **1995**, *34*, 4979−4985.
(45) Jourdain, I. V.; Fourmigué, M.; Guyon, F.; Amaudrut, J. *J. Chem. Soc., Dalton Trans.* **1998**, 483−488.
(46) Green, M. L. H.; Heuer, W. B.; Saunders, G. C. *J. Chem. Soc., Dalton Trans.* **1990**, 3789−3792.
(47) Pilato, R. S.; Eriksen, K. A.; Greaney, M. A.; Stiefel, E. I.; Goswami, S.; Kilpatrick, L.; Spiro, T. G.; Taylor, E. C.; Rheingold, A. L. *J. Am. Chem. Soc.* **1991**, *113*, 9372−9374.
(48) Würthner, F. *Chem. Commun.* **2004**, 1564−1579.
(49) Vân Anh, N.; Schlosser, F.; Groeneveld, M. M.; van Stokkum, I. H. M.; Würthner, F.; Williams, R. M. *J. Phys. Chem. C* **2009**, *113*, 18358−18368.
(50) Hippius, C.; Schlosser, F.; Vysotsky, M. O.; Böhmer, V.; Würthner, F. *J. Am. Chem. Soc.* **2006**, *128*, 3870−3871.
(51) Lukas, A. S.; Zhao, Y.; Miller, S. E.; Wasielewski, M. R. *J. Phys. Chem. B* **2002**, *106*, 1299−1306.
(52) Tauber, M. J.; Kelley, R. F.; Giaimo, J. M.; Rybtchinski, B.; Wasielewski, M. R. *J. Am. Chem. Soc.* **2006**, *128*, 1782−1783.
(53) Gunderson, V. L.; Krieg, E.; Vagnini, M. T.; Iron, M. A.; Rybtchinski, B.; Wasielewski, M. R. *J. Phys. Chem. B* **2011**, *115*, 7533−7540.
(54) Flamigni, L.; Ventura, B.; Barbieri, A.; Langhals, H.; Wetzel, F.; Fuchs, K.; Walter, A. *Chem.—Eur. J.* **2010**, *16*, 13406−13416.
(55) Mikroyannidis, J. A.; Stylianakis, M. M.; Suresh, P.; Sharma, G. D. *Sol. Energy Mater. Sol. Cells* **2009**, *93*, 1792−1800.
(56) Goretzki, G.; Davies, E. S.; Argent, S. P.; Warren, J. E.; Blake, A. J.; Champness, N. R. *Inorg. Chem.* **2009**, *48*, 10264−10274.
(57) Chamberlain, T. W.; Davies, E. S.; Khlobystov, A. N.; Champness, N. R. *Chem.—Eur. J.* **2011**, *17*, 3759−3767.
(58) Bhosale, S. V.; Jani, C. H.; Langford, S. J. *Chem. Soc. Rev.* **2008**, *37*, 331−342.
(59) Gosztola, D.; Niemczyk, M. P.; Svec, W.; Lukas, A. S.; Wasielewski, M. R. *J. Phys. Chem. A* **2000**, *104*, 6545−6551.
(60) Chernick, E. T.; Mi, Q.; Vega, A. M.; Lockard, J. V.; Ratner, M. A.; Wasielewski, M. R. *J. Phys. Chem. B* **2007**, *111*, 6728−6737.
(61) Flamigni, L.; Ventura, B.; You, C.-C.; Hippius, C.; Würthner, F. *J. Phys. Chem. C* **2007**, *111*, 622−630.
(62) Sazanovich, I. V.; Alamiry, M. A. H.; Best, J.; Bennett, R. D.; Bouganov, O. V.; Davies, E. S.; Grivin, V. P.; Meijer, A. J. H. M.; Plyusnin, V. F.; Ronayne, K. L.; Shelton, A. H.; Tikhomirov, S. A.; Towrie, M.; Weinstein, J. A. *Inorg. Chem.* **2008**, *47*, 10432−10445.
(63) Shavaleev, N. M.; Davies, E. S.; Adams, H.; Best, J.; Weinstein, J. A. *Inorg. Chem.* **2008**, *47*, 1532−1547.
(64) Bhosale, S. V.; Jani, C. H.; Langford, S. J. *Chem. Soc. Rev.* **2008**, *37*, 331−342. Aveline, B. M.; Matsugo, S.; Redmond, R. W. *J. Am. Chem. Soc.* **1997**, *119*, 11785−11795. McMasters, S.; Kelly, L. A. *J. Phys. Chem. B* **2006**, *110*, 1046−1055. Kawai, K.; Osakada, Y.; Fujitsuka, M.; Majima, T. *J. Phys. Chem. B* **2007**, *111*, 2322−2326. Rogers, J. E.; Kelly, L. A. *J. Am. Chem. Soc.* **1999**, *121*, 3854−3861.

Ryan, G. J.; Quinn, S.; Gunnlaugsson, T. *Inorg. Chem.* **2008**, *47*, 401−403.
(65) Weiss, E. A.; Sinks, L. E.; Lukas, A. S.; Chernick, E. T.; Ratner, M. A.; Wasielewski, M. R. *J. Phys. Chem. B* **2004**, *108*, 10309−10316.
(66) Tunney, J. M.; Blake, A. J.; Davies, E. S.; McMaster, J.; Wilson, C.; Garner, C. D. *Polyhedron* **2006**, *25*, 591−598.
(67) Bruce, A. E.; Bruce, M. R. M.; Sclafani, A.; Tyler, D. R. *Organometallics* **1984**, *3*, 1610−1614.
(68) Andric, G.; Boas, J. F.; Bond, A. M.; Fallon, G. D.; Ghiggino, K. P.; Hogan, C. F.; Hutchison, J. A.; Lee, M. A.-P.; Langford, S. J.; Pilbrow, J. R.; Troup, G. J.; Woodward, C. P. *Aust. J. Chem.* **2004**, *57*, 1011−1019.
(69) Kilpatrick, L.; Rajagopalan, K. V.; Hilton, J.; Bastian, N. R.; Stiefel, E. I.; Pilato, R. S.; Spiro, T. G. *Biochemistry* **1995**, *34*, 3032−3039.
(70) Subramanian, P.; Burgmayer, S.; Richards, S.; Szalai, V.; Spiro, T. G. *Inorg. Chem.* **1990**, *29*, 3849−3853.
(71) Schläpfer, C. W.; Nakamoto, K. *Inorg. Chem.* **1975**, *14*, 1338−1344.
(72) Elsaesser, T.; Kaiser, W. *Annu. Rev. Phys. Chem.* **1991**, *42*, 83−107.
(73) Adams, C. J.; Fey, N.; Harrison, Z. A.; Sazanovich, I. V.; Towrie, M.; Weinstein, J. A. *Inorg. Chem.* **2008**, *47*, 8242−8257.
(74) (a) Ganesan, P.; Baggerman, J.; Zhang, H.; Sudhölter, E. J. R.; Zuilhof, H. *J. Phys. Chem. A* **2007**, *111*, 6151−6156. (b) Weiss, E. A.; Ahrens, M. J.; Sinks, L. E.; Gusev, A. V.; Ratner, M. A.; Wasielewski, M. R. *J. Am. Chem. Soc.* **2004**, *126*, 5577−5584. (c) Daub, J.; Engl, R.; Kurzawa, J.; Miller, S. E.; Schneider, S.; Stockmann, A.; Wasielewski, M. R. *J. Phys. Chem. A* **2001**, *105*, 5655−5665. (d) Greenfield, S. R.; Svec, W. A.; Gosztola, D.; Wasielewski, M. R. *J. Am. Chem. Soc.* **1996**, *118*, 6767−6777. (e) Johansson, O.; Borgstrom, M.; Lomoth, R.; Palmblad, M.; Bergquist, J.; Hammastrom, L.; Sun, L.-C.; Akermark, B. *Inorg. Chem.* **2003**, *42*, 2908−2918. (f) Hanss, D.; Walther, M. E.; Wenger, O. S. *Coord. Chem. Rev.* **2010**, *254*, 2584−2592.
(75) Kolosov, D.; Adamovich, V.; Djurovich, P.; Thompson, M. E.; Adachi, C. *J. Am. Chem. Soc.* **2002**, *124*, 9945−9954.
(76) Leedy, D. W.; Muck, D. L. *J. Am. Chem. Soc.* **1971**, *93*, 4264−4270.
(77) Green, S.; Fox, M. A. *J. Phys. Chem.* **1995**, *99*, 14752−14757.
(78) Rogers, J. E.; Kelly, L. A. *J. Am. Chem. Soc.* **1999**, *121*, 3854−3861.
(79) Flamigni, L.; Baranoff, E.; Collin, J. P.; Sauvage, J. P. *Chem.—Eur. J.* **2006**, *12*, 6592−6606.
(80) Hayes, R. T.; Wasielewski, M. R.; Gosztola, D. *J. Am. Chem. Soc.* **2000**, *122*, 5563−5567.
(81) Macgregor, S. A.; McInnes, E.; Sorbie, R. J.; Yellowlees, L. J. *Molecular Electrochemistry of Inorganic, Bioinorganic and Organometallic Compounds*; Pomberio, A. J. L., McCleverty, J. A., Eds.; Kluwer Academic Publishers: Dordrecht, The Netherlands, 1993; p 503.
(82) Blokhin, A. P.; Gelin, M. F.; Buganov, O. V.; Dubovskii, V. A.; Tikhomirov, S. A.; Tolstorozhev, G. B. *J. Appl. Spectrosc.* **2003**, *70*, 70−78.
(83) Greetham, G. M.; Burgos, P.; Cao, Q.; Clark, I. P.; Codd, P. S.; Farrow, R. C.; George, M. W.; Kogimtzis, M.; Matousek, P.; Parker, A. W.; Pollard, M. R.; Robinson, D. A.; Xin, Z.-J.; Towrie, M. *Appl. Spectrosc.* **2010**, *64*, 1311−1319.
(84) Guerra, C. F.; Snijders, J. G.; te Velde, G.; Baerends, E. J. *Theor. Chem. Acc.*, 1998, *99*, 391−403; *ADF 2000.02, 2004.01 and 2005.1*; SCM, Vrijie Unversiteit: Amsterdam, The Netherlands, www.scm.com; te Velde, G.; Bickelhaupt, F. M.; Baerends, E. J.; Guerra, C. F.; Van Gisbergen, S. J. A.; Snijders, J. G.; Ziegler, T. *J. Comput. Chem.* **2001**, *22*, 931−967.
(85) van Lenthe, E.; Baerends, E. J.; Snijders, J. G. *J. Chem. Phys.* **1993**, *99*, 4597−4610; **1994**, *101*, 9783−9792. Wolff, S. K.; Ziegler, T.; van Lenthe, E.; Baerends, E. J. *J. Chem. Phys.* **1999**, *110*, 7689−7698. van Lenthe, E.; Ehlers, A.; Baerends, E. J. *J. Chem. Phys.* **1999**, *110*, 8943−8953.
(86) Vosko, S. H.; Wilk, L.; Nusair, M. *Can. J. Phys.* **1980**, *58*, 1200−1211.
(87) Becke, A. D. *Phys. Rev. A.* **1988**, *38*, 3098−3100.
(88) Perdew, J. P. *Phys. Rev. B* **1986**, *33*, 8822−8824.
(89) Flükiger, P. F. Ph.D. Thesis, Université de Genève, Geneva, Switzerland, 1992; Portmann, S.; Luthi, H. P. *Chimia* **2000**, *54*, 766−770.
(90) Gorelsky, S. I. *SWizard program*; University of Ottawa: Ottawa, Canada, 2010; http://www.sg-chem.net/.
(91) Merkel, P. B.; Luo, P.; Dinnocenzo, J. P.; Farid, S. *J. Org. Chem.* **2009**, *74*, 5163−5173.